RL-TR-96-63
Final Technical Report
April 1996

ADVANCED QUANTUM WELL OPTOELECTRONICS FOR OPTICALLY CONTROLLED PHASED-ARRAY SYSTEMS

University of California, Berkeley

Sponsored by
Advanced Research Projects Agency

APPROVED FOR PUBLIC RELEASE; DISTRIBUTION UNLIMITED.

Rome Laboratory
Air Force Materiel Command
Rome, New York

This report has been reviewed by the Rome Laboratory Public Affairs Office (PA) and is releasable to the National Technical Information Service (NTIS). At NTIS it will be releasable to the general public, including foreign nations.

RL-TR-96-63 has been reviewed and is approved for publication.

APPROVED: Richard A Soref

DR. RICHARD A. SOREF
Project Engineer

FOR THE COMMANDER: Robert V. McGahan

ROBERT V. MCGAHAN
Director
Electromagnetics & Reliability Directorate

If your address has changed or if you wish to be removed from the Rome Laboratory mailing list, or if the addressee is no longer employed by your organization, please notify RL (EROC) Hanscom AFB MA 01731. This will assist us in maintaining a current mailing list.

Do not return copies of this report unless contractual obligations or notices on a specific document require that it be returned.

ADVANCED QUANTUM WELL OPTOELECTRONICS FOR OPTICALLY CONTROLLED PHASED-ARRAY SYSTEMS

Kam Y. Lau

Contractor: University of California, Berkeley
Contract Number: F19628-91-K-0006
Effective Date of Contract: 06 December 1991
Contract Expiration Date: 30 September 1995
Short Title of Work: Advanced Quantum Well Optoelectronics for Optically Controlled Phased-Array Systems
Period of Work Covered: Jan 91 - Sep 95

Principal Investigator: Kam Y. Lau
Phone: (510) 642-6251

RL Project Engineer: Dr. Richard A. Soref
Phone: (617) 377-2380

This research was supported by the Advanced Research Projects Agency of the Department of Defense and was monitored by Dr. Richard A. Soref, RL/EROC, 80 Scott Rd, Hanscom AFB MA 01731-2909.

REPORT DOCUMENTATION PAGE

Form Approved
OMB No. 0704-0188

1. AGENCY USE ONLY (Leave Blank)	2. REPORT DATE	3. REPORT TYPE AND DATES COVERED
	April 1996	Final Jan 91 - Sep 95

4. TITLE AND SUBTITLE

ADVANCED QUANTUM WELL OPTOELECTRONICS FOR OPTICALLY CONTROLLED PHASED-ARRAY SYSTEMS

5. FUNDING NUMBERS

C - F19628-91-K-0006
PE - 61101E
PR - G310
TA - AR
WU - 20

6. AUTHOR(S)

Kam Y. Lau

7. PERFORMING ORGANIZATION NAME(S) AND ADDRESS(ES)

University of California, Berkeley
Electronics Research Laboratory
253 Cory Hall
Berkeley CA 94720

8. PERFORMING ORGANIZATION REPORT NUMBER

N/A

9. SPONSORING/MONITORING AGENCY NAME(S) AND ADDRESS(ES)

Advanced Research Projects Agency
3701 North Fairfax Drive
Arlington VA 22203-1714

Rome Laboratory/EROC
80 Scott Rd
Hanscom AFB MA 01731-2909

10. SPONSORING/MONITORING AGENCY REPORT NUMBER

RL-TR-96-63

11. SUPPLEMENTARY NOTES

Rome Laboratory Project Engineer: Dr. Richard A. Soref/EROC/(617) 377-2380

12a. DISTRIBUTION/AVAILABILITY STATEMENT

Approved for public release; distribution unlimited.

12b. DISTRIBUTION CODE

13. ABSTRACT (Maximum 200 words)

During the course of this effort, the researcher successfully completed experimental and theoretical investigations of three techniques used to transmit narrowband millimeter (mm-wave) analog signals over optical fiber: 1) narrowband mm-wave optical transmitters based on resonant modulation of monolithic semiconductor lasers; 2) feedforward optical modulation; and 3) a passively mode-locked laser operating in an optoelectronics phase-locked loop.

14. SUBJECT TERMS

Modulation efficiency, Passband bandwidth, Noise and intermodulation distortion

15. NUMBER OF PAGES

56

16. PRICE CODE

17. SECURITY CLASSIFICATION OF REPORT	18. SECURITY CLASSIFICATION OF THIS PAGE	19. SECURITY CLASSIFICATION OF ABSTRACT	20. LIMITATION OF ABSTRACT
UNCLASSIFIED	UNCLASSIFIED	UNCLASSIFIED	UL

TABLE OF CONTENTS

Summary

During the course of this contract, we have successfully completed experimental and theoretical investigations of three techniques used to transmit narrowband millimeter wave (mm-wave) analog signals over optical fiber: 1) narrowband mm-wave optical transmitters based on resonant modulation of monolithic semiconductor lasers, (2) feedforward optical modulation, and (3) a passively mode-locked laser operating in an optoelectronic phase-locked loop. The resonant modulation response at the cavity round-trip frequency is fully characterized for multiple-contact lasers under various bias conditions. Issues such as modulation efficiency, passband bandwidth, noise and intermodulation distortion are addressed. A system implementation of resonant modulation is presented in which two simultaneous 2.5Mb/s BPSK channels centered at a subcarrier frequency of 41GHz is transmitted over 400 meters of single-mode fiber. Simple microstrip matching circuits are fabricated at 41GHz to couple the mm-wave signals into the laser. Resonant modulation of single-contact lasers is also reported. Next, implementation of a tunable mm-wave (30-300GHz) optical transmitter based on feedforward optical modulation is presented, and the fundamental performance of this technique investigated in terms of noise and dynamic range. Feedforward modulation is used to transmit 300Mb/s data at 39GHz over 2.2km of single-mode fiber. Finally, a passively mode-locked monolithic semiconductor laser operating in an optoelectronic phase-locked loop is implemented as a narrowband mm-wave optical transmitter at 46GHz. The phase-locked loop bandwidth, mm-wave tracking capability, and fundamental limit to the stability of the mm-wave subcarrier is established. The relative merits of the three techniques are discussed and compared. The mm-wave subcarrier transmission results presented here are the highest reported to date.

I. INTRODUCTION

Optical fiber links capable of efficiently transporting mm-wave (>30GHz) signals in applications such as indoor mm-wave fiber-fed picocellular networks, wireless mm-wave cable-television systems and phased-array antenna networks has recently attracted considerable interest [1]-[6]. Future deployment of a fiber infrastructure in these systems rests primarily upon the availability of low-cost mm-wave optical transmitters. Semiconductor quantum-well laser with a direct modulation bandwidth of 30GHz has been demonstrated [7], but it remains unclear what the prospects are for semiconductor lasers with direct modulation bandwidths exceeding 30GHz. Traveling-wave external modulators with electrical bandwidths exceeding 35GHz have been reported, but suffer from high optical insertion loss, high drive voltage and aging [8,9]. Noting that most mm-wave applications require only a relatively narrow bandwidth centered at a high frequency, alternate means have been and are currently being pursued which bypass the direct modulation bandwidth limitations of existing devices. One method uses active mode-locking of a semiconductor laser coupled to an external cavity, creating a narrowband resonantly enhanced transmission window at multiples of the cavity round-trip frequency [10, 11]. Transmission of a single channel at 40Mb/s centered at a subcarrier frequency of 35GHz was demonstrated using this technique [12]. Monolithic semiconductor lasers, on the other hand, have typical cleaved lengths leading to intermodal frequencies in the mm-wave region [13,14]. This makes it possible for simple, efficient mm-wave optical transmitters to be built having a narrowband ($\leq$1GHz) modulation response centered at frequencies up to 100GHz [14, 15]. Optical transmission of a single, narrowband (50Mb/s) channel at 45GHz was demonstrated using resonant modulation of a low-frequency (direct modulation bandwidth <5GHz) multiple-contact solitary semiconductor laser diode [15].

Feedback approaches combining optical heterodyning and optoelectronic phase-locked loops have also been considered for transmitting narrowband microwave and mm-wave subcarriers [16,17]. It is inherently difficult to extend the bandwidth of any feedback technique much

beyond 100 MHz due to feedback delay. Precise control of the feedback delay has led to a phase-locked loop bandwidth of 180MHz at 18GHz [16]. In a previous letter, we reported implementation of a narrowband optoelectronic phased-locked loop to stabilize the intensity oscillations of a passively mode-locked laser at 41GHz [18]. Feedforward, as opposed to feedback error correction, has also been investigated. Feedforward modulators eliminate the bandwidth limitations inherent in feedback techniques such as phase-locked loops. A tunable mm-wave transmitter based on feedforward error correction was recently reported [19].

In this report, we describe in detail and compare the performance of mm-wave optical transmitters based on resonant modulation of monolithic semiconductor lasers, feedforward modulation, and a passively mode-locked laser operating in an optoelectronic phase-locked loop. Emphasis is placed on system issues related to narrowband resonant modulation using monolithic semiconductor laser diodes. In section II, the modulation response and two-tone dynamic range of multiple-contact semiconductor lasers is characterized as a function of bias at the cavity round-trip frequency. We discuss details of a multichannel system implementation of resonant modulation in which two signals centered around 41GHz with 2.5Mb/s BPSK data are transmitted over 400 meters of optical fiber. Resonant modulation of single-contact laser structures is also demonstrated. In Section III, we describe the implementation of a mm-wave optical transmitter based on feedforward optical modulation and establish the limits to this technique in terms of noise and dynamic range. Details of a subcarrier lightwave link transmitting 300Mb/s data at 39GHz using feedforward modulation is discussed. Section IV considers the use of a simple optoelectronic phase-locked loop with external optical feedback to stabilize the intensity oscillations at 46GHz out of an uncoated monolithic passively mode-locked laser diode. The fundamental limit of this technique in terms of phase noise of the mm-wave subcarrier and dynamic range is considered. The relative merits of the three techniques are discussed and summarized in Section V.

II. RESONANT MODULATION

A. Principle and Analysis

Figure 1 illustrates the principle of resonant modulation. The modulation response for both the low and high frequency ranges of a multiple-contact GaAs quantum-well laser diode emitting at 850nm with a cavity length L~820μm is shown. In the low frequency range, the response drops off beyond a few gigahertz which is typical of a device of this cavity length. At the cavity round-trip resonant frequency of $f_{RT} = c/(2n_g L) = 45$ GHz, the response peaks up sharply due to the coupling of longitudinal modes resulting from the applied modulation signal. This greatly enhanced narrowband transmission window in the modulation response is used to efficiently transmit mm-wave signals over optical fiber. The response can be further enhanced by incorporating a saturable absorber section. By adjusting the bias voltage to the absorber, the peak response can be made higher than that of the conventional low-frequency response. Figure 1 shows that the modulation efficiency at 45GHz is >10dB higher than that of a conventional device at d.c. (below relaxation oscillation). The higher modulation efficiency is, however, achieved at the expense of passband bandwidth. A maximum bandwidth of 300MHz is obtained under homogeneous current bias, as shown in Figure 1. The noise is also higher for the situation corresponding to a higher modulation efficiency, since the device is now approaching the passively mode-locked regime and begins to self-oscillate at the resonant round-trip frequency. As indicated in [14, 15], the noise is not a constant additive noise as in a conventional laser intensity noise, but is dependent on the applied modulation signal power due to injection-locking effects. This is illustrated in Figure 2, where the carrier-to-noise ratio (CNR) is plotted against absorber bias voltage for two input RF drive powers at a subcarrier frequency of 45GHz. Note that a 3dB increase in RF drive power results in a 4 to 8 dB improvement in the CNR, depending on the bias conditions. The inset shows the suppression of the noise by~7dB at 45GHz due to injection locking for an absorber bias voltage of V_a =-0.44V. For resonant modulation, CNR values as high as 100dB(1 Hz) have been observed.

The basic approach to describe phenomena related to modulation at or near the cavity round-trip frequency is based on coupling between longitudinal modes---the common mode-lock-

ing approach in the frequency domain [20]. Details of the analysis is provided in Refs. [13, 14]. The standard mode-coupling equations are [14, 20]:

$$A_k\left[\left(ik\delta - \frac{1}{2\tau_p}\right)\frac{1}{g_k} + \frac{n_o G}{2}\right] = \frac{-nG\xi}{2}\left(A_{k-1} + A_{k+1}\right) \tag{1}$$

where the A_k's are longitudinal mode amplitudes, τ_p , G, and g_k are, respectively, the photon lifetime, differential gain of the mode at the center of the (parabolic) gain spectrum, and the relative differential gain of the k mode, with the form $g_k = 1/(1+b^2k^2)$; $= \Omega - \Omega_o$ is the detuning of the applied modulation frequency (Ω) from the intermodal separation (Ω_o), assumed to be constant (no dispersion). The electron density is assumed to take the form

$$N(r,t) = n_o + F(\vec{r})\,2n\cos\Omega t \ , \tag{2}$$

where a uniform bias over the cavity and modulation is applied only to part of it [$F(\vec{r})$]. The factor ξ in Eq. (1) is the spatial overlap integral between $F(\vec{r})$ and two neighboring longitudinal modes, and is given by $\xi = \int F(\vec{r})\,u_k(\vec{r})\,u_{k+1}(\vec{r})\,d\vec{r}$. Letting the photon density vary as $(t) = S_o(1+p\cos[\Omega t])$, an analytic solution for the optical modulation depth for homogeneous bias is given as [13, 14]:

$$p = \frac{4G\tau_p\xi n}{b^2 - 2i\tau_p\delta} \tag{3}$$

The quantity b is the modal discrimination factor, and is the ratio of the intermodal frequency spacing to the effective width of the gain spectrum $b = \Omega_o/\omega_g$. To relate n to the applied modulation current j_a, we use Eq. (3) in the standard small-signal electron rate equation and

solve self-consistently, yielding the response for homogenous bias [14]:

$$p/j_a = \frac{4G\tau_p\xi}{\left(2\xi GS_o + 2\tau_p\Omega\delta + \frac{b^2}{\tau_s}\right) + i\left(\Omega b^2 - 2\frac{\tau_p}{\tau_s}\delta\right)} \tag{4}$$

The magnitude of this response function is plotted in Figure 3 at $\Omega_o = 2\pi 45$GHz and at 94 GHz with the varying parameter in each plot being *b*. In a plain laser cavity, *b* is determined by the material gain spectral width, however, it is possible to vary $_g$ by incorporating intracavity frequency selective elements such as gratings or coupled cavities. Resonant modulation of a 1.55μm three-section Distributed Bragg Reflector (DBR) laser was demonstrated recently, and control of *b* was accomplished by varying the current into the Bragg section [21].

Figures 1 and 3 also reveal that substantial improvement in the modulation efficiency is accomplished by inhomogeneously biasing the laser. The enhancement in the modulation efficiency is a consequence of the nonlinear gain characteristic of quantum-well lasers. The modulation response under inhomogeneous bias is obtained by performing an analysis very similar to that of the homogeneous bias case. Equation (3) is modified to take into account the electron density rate equation of the absorber [22]. A simple expression for the enhancement in the modulation efficiency of the inhomogeneously biased device over its homogeneous counterpart when modulating the shorter (absorbing) section can be obtained by evaluating the ratio of the inhomogeneous response function $\left(p/j_a\right)_{IH}$ to the homogeneous response $\left(p/j_a\right)_H$ near the resonant peak Ω_o for each biasing scheme. The result is:

$$\eta = \left|\frac{\left(p/j_a\right)_{IH}}{\left(p/j_a\right)_H}\right|^2_{\omega \approx \Omega_o} \approx \left(\frac{G_a}{G}\right)^2 \tag{5}$$

where G_a is the differential gain of the absorber section of the inhomogeneously biased device and G is the differential gain of the homogeneously biased device (in m^3s^{-1}). Values of G_a/G as high as 10 have been reported [23], leading to a 20dB enhancement in the modulation efficiency for inhomogeneous bias. The calculated response functions for inhomogeneous bias are also plotted in Figure 3 for a typical ratio of G_a/G =7. There is good agreement between these analytical results and the experimental results of Figure 1 for modal discrimination factor $b \sim 0.1$. The passband bandwidth for both biasing schemes is given by $BW = b^2/\left(4\pi\tau_p\right)$, or approximately 1% -2% of the center frequency for typical values of b. Note that a shift in the peak of the response function is observed in both Figures 1 and 3. Furthermore, it can be shown that the increase in the modulation efficiency is accompanied by a corresponding increase in the noise of only G_a/G , and a comparable decrease in the signal-to-intermodulation distortion ratio [22].

B. Dynamic Range and Millimeter Wave Matching Circuits

To ascertain the dynamic range of resonantly modulated multiple-contact Fabry-Perot lasers, we use the setup illustrated in Figure 4. The cavity-round trip frequency for the laser used here is 41GHz. Two-tone measurements are performed by first power combining the output of two Gunn oscillators emitting at 41GHz and separated by ~1MHz. Electrical isolation between the oscillators is >30dB. The signals are delivered to the laser with the aid of a single-section microstrip matching circuit having a magnitude reflection coefficient $|S_{11}|$ shown in Figure 5. Laser package and impedance measurements were obtained with an 8510C network analyzer and fed into Touchstone to design the matching circuit. Trimming of the microstrip board was done to obtain a narrowband match at 41GHz. A Wiltron 3680V 50GHz test fixture is used to hold the board and provide a matched transition between the microstrip board and Wiltron V-connectors. The power emitted from the laser is sent through 400 meters of single-mode fiber at 850nm where it is detected, downconverted to IF and observed on a spectrum analyzer. The resulting dynamic range plot is shown in Figure 6a. At a modulation efficiency of -5dB (relative to that below

relaxation oscillation), a two-tone spur-free dynamic range of 66dB-$Hz^{2/3}$ is obtained for this conventional Fabry-Perot laser. It was also observed that one can trade off modulation efficiency for dynamic range. Other structures that incorporate intracavity frequency selective elements such as gratings are predicted to have a higher dynamic range at the expense of modulation efficiency [14]. Figure 6b shows the output of a two-tone test of a tunable three-section DBR laser at ~45GHz. The dynamic range for this laser was measured to be 75dB-$Hz^{2/3}$ [21]. Although 75dB-$Hz^{2/3}$ is insufficient for conventional AM cable-television systems; it was shown that for a voice channel bandwidth of 30kHz, this dynamic range is adequate for supporting up to 5 frequency channels in a wireless microcell with only a 2.5% probability of blocked calls [24].

C. System Implementation of Resonant Modulation

Next, the performance of the transmitter modulated by two binary-phase shift-keyed (BPSK) subcarrier channels is ascertained using the same setup illustrated in Figure 4. The laser is biased for a modulation efficiency of ~0dB (relative to d.c), a passband bandwidth of ~200MHz, and an optical power of ~2mW. Two channels, each transmitting pseudorandom(2^9-1) return-to-zero data at 2.5Mb/s are upconverted to 41GHz using a Q-band waveguide mixer and power combined to modulate the laser. The signals are transmitted over 400 meters of single-mode fiber. At the receiver, the signals are down-converted to baseband, amplified and sent to an error-rate tester. The BER vs. electrical drive power of channel 1 (centered at ~41.15GHz) is first measured with channel 2 (centered at ~40.95GHz) turned off as shown in Figure 7. The required RF power drive power to the laser to achieve a BER of 10^{-9} for this single channel is -2.5dBm. With channel 2 activated, an additional 2dB of RF power (RF power penalty) is required to keep channel 1 operating at 10^{-9}. Likewise, the drive power required for channel 2 to operate at 10^{-9} in the presence of channel 1 is 5dBm. The difference in RF power between the channels for 10^{-9} operation stems from injection-locking effects which occur under higher RF drive power. As illustrated in the inset of Figure 7, the signal RF power at channel 1 leads to a higher level of noise at channel 2 due to injection-locking effects. At lower drive powers, both channels act independently as evidenced by the convergence of the BER curves at low drive powers. The effect on the BER as the RF channel

spacing is varied is the subject of further investigation [25]. Based on these transmission results and by taking advantage of conventional wireless time-division multiplexing techniques in which up to 8 users can share a single channel [1], mm-wave links based on resonant modulation are adequate for remoting signals from an antenna serving up to 16 mobile users in an indoor environment.

D. Single-Contact Devices

For resonant modulation to occur, the modulating signal must be applied to only a part of the laser cavity, as designated by the factor $F(\vec{r})$ in (2) above. This is typically facilitated by splitting the contact of the laser. Recently, it was suggested that the propagation loss of an applied high-frequency modulation signal along the contact of the laser may be significant and needs to be considered at frequencies >20GHz [26]. In this section, we show that we can take advantage of the microwave propagation loss of the applied modulation signal along the contact of the laser to obtain resonant modulation of a *single-contact* semiconductor diode laser at a cavity round-trip frequency of ~40GHz [27]. This is highly significant since a conventional single-contact device can now be used to perform resonant modulation or ultrahigh frequency mode-locking. This can considerably simplify the design of narrowband millimeter wave transmitters based on resonant modulation of monolithic semiconductor lasers. In this section, the optical modulation efficiency at the cavity round-trip frequency is studied as the modulation is introduced at various points along the contact of the laser.

Figure 8a illustrates the principle. The inherent microwave propagation loss (~60dB/mm at 40GHz) along the contact of the laser confines the signal current in a narrow region near the launch point. Confinement of the current at high frequencies eliminates the need for a second contact. Modulation response measurements were performed on a conventional coplanar ridge-waveguide laser diode emitting at 1μm with a cavity length L ~ 1mm, corresponding to an intermodal frequency spacing of 40.2GHz. The modulation signal is launched into the laser via a coplanar (ground-signal-ground) microwave probe having a bandwidth of 40GHz. The modula-

tion response in the vicinity of the cavity round-trip frequency is obtained by sweeping a tunable mm-wave oscillator. Modulation response measurements at two probe positions along the contact of the laser is shown in Figure 8b. For this laser, a modulation efficiency of -20dB relative to that at low frequencies (below relaxation oscillation) was observed when the probe is placed at *L/4* from either edge (facet) of the laser. This is comparable to that obtained with split-contact monolithic laser structures under homogeneous bias.

The optical modulation response given in (4) also applies to single-contact devices, the only difference being the interpretation of the spatial overlap integral ξ, also defined above. We assume that the photon density is small such that the spatial dependence of the gain modulation $F(\vec{r})$ can be approximated by the injection current $I(\vec{r})$. The quantity ξ is then given by $\xi = \frac{1}{L}\int_0^L I(z)\cos\left(\frac{\pi z}{L}\right)dz$ and is plotted here in Figure 9 as a function of probe position along the contact. The quantity L is the length of the laser and $I(z)$ is the normalized spatial dependence of the modulation current. Only the longitudinal direction is considered. It is assumed that the modulation current propagating along the cavity attenuates according to a standard distributed open-ended (with two open ends) transmission line circuit model shown in the inset of Figure 9, with an impedance $Z = Z_o \coth(\gamma l)$. The quantity γ is the complex propagation constant, and l is the distance from the feed point to the nearest open end (facet). The model predicts that the modulation efficiency is a maximum when probing at a location approximately *L/8* from the edge of the laser. The plot also shows ξ calculated by assuming for simplicity the modulation current confined to a delta-function along the contact (infinite propagation loss), and is a good approximation to the standard transmission line model (with finite loss). The spatial overlap and hence the modulation efficiency is zero when the probe is positioned exactly at the center of the cavity.

III. FEEDFORWARD MODULATION

A. Principle and Analysis

Resonant modulation was considered in the last section as a means of constructing simple narrowband mm-wave optical transmitters using conventional monolithic semiconductor laser diodes. However, once the device length is fixed, the passband frequency cannot be varied. Some mm-wave applications, however, require that the center frequency vary over a wide range (e.g. frequency hopping). In this section, a technique is described for mm-wave optical modulation where the operational frequency band can be easily tuned over a span of tens of GHz. No high frequency optoelectronic components are required, with the exception of a high speed photodetector (which is a required component in any case for the mm-wave receiver at the end of the fiber link). The technique is based on the tunable beat note generated by photomixing of two single frequency laser diodes. Attempts have been made in the past to use the photomixed beat note as a variable frequency RF signal source, but the instability of the beat note due to the intrinsic phase noise of the lasers, as well as extrinsic factors, remains an issue for laser diodes and for diode-pumped YAG lasers. In any event, the beat note so generated is a relatively noisy RF-carrier (modulated on an optical beam) that must be encoded with the signal one intends to transmit. An established method to achieve this is through the use of a phase-locked loop, although it is inherently difficult to extend the bandwidth of any feedback technique much beyond 100 MHz. The technique reported here begins with a noisy photomixed optical beat note, and, through the use of feedforward compensation, impresses the mm-wave signal on the optical beam. The ability of this approach to transmit data with high fidelity will require, in addition to having adequate small-signal bandwidth, good distortion characteristics under large signal modulation. Transmission of 300 Mb/s BPSK data at a carrier frequency of 39GHz over 2.2km of single-mode fiber is demonstrated. Furthermore, these results indicate that gigabit-per-second rates at subcarrier frequencies extending to 100 GHz and beyond is possible using this technique.

The operational principle of the feedforward optical modulation technique is illustrated in Fig. 10. If we express the electric field out of each DFB laser as

$$E_{1,2}(t) = A_{1,2} e^{i\left[\omega_{1,2} t + \phi_{1,2}(t)\right]} \tag{6}$$

where A is the field amplitude, ω the optical frequency and ϕ the time dependent phase fluctuations that arises from the finite linewidth of the lasers, then the intensity propagating in the fibers after the coupler is

$$= I_o\left[1 + k\cos\left(\omega_B t + \Theta(t)\right)\right] \tag{7}$$

where $k = 2A_1A_2/(A_1^2 + A_2^2)$ is the modulation depth of the beat note, ω_B is the beat note radian frequency and $\Theta(t)$ is the stochastic beat-note phase. One of the outputs from the coupler is detected by a standard high speed photodetector and the beat note is mixed with the input mm-wave signal to be transmitted, which, for the purpose of this analysis, is assumed to be a sine wave at the frequency ω_{MM} as shown in Figure 10. The laser optical frequencies are adjusted so that ω_B is close to, but not exactly equal to ω_{MM}. The down converted signal is filtered, amplified and sent to the electrical input of a low-frequency (BW < 5GHz) external modulator that modulates the light from the other coupler output. The external modulator only has to respond to the low frequency down converted signal, *not* the high frequency mm-wave input. Assuming the modulator is operated in the linear region, its output intensity can be expressed as [19]:

$$I_{out} = \frac{I_o}{2}\Big(1 + k\cos\left[\omega_B t + \Theta(t)\right] - m\cos\left[\left(\omega_B - \omega_{MM}\right)t + \Theta(t+\tau)\right]$$

$$-\frac{km}{2}\Big(\cos\left[\left(2\omega_B - \omega_{MM}\right)t + \Theta(t+\tau) + \Theta(t)\right] + \cos\left[\omega_{MM}t + \Theta(t) - \Theta(t+\tau)\right]\Big)\Big) \tag{8}$$

where I_o is the optical intensity at the external modulator input, m is the RF modulation depth into the external modulator, τ is the difference in time delay of the two paths from the coupler to the

external modulator, and ω_{MM} is the angular frequency of the input signal. The intensity spectrum of (8) has four components: the low frequency down converted signal (ω_B-ω_{MM}), the beat note (ω_B), a mixer product at $2\omega_B$-ω_{MM} and a replica of the input signal (ω_{MM}), all delineated in Figure 10. This last component at ω_{MM} is the desired signal that we intend to transmit. The others will be filtered out, either by optical or electrical means, at the receiver.

The first and last terms in (8) give rise to two additional noise terms unique to the feedforward modulator (other than the standard shot and thermal noise which are present in all analog links. The laser relative-intensity-noise (RIN) is not included here since we are operating well above the relaxation frequency of the lasers). The first term is the beat note ω_B, which lies adjacent to the signal frequency ω_{MM}. The Lorentzian tail of the beat note ω_B extends into the frequency band occupied by the signal ω_{MM}, and appears as an additional source of white noise within the signal bandwidth. This is illustrated in Figure 11, which shows a spectrum analyzer measurement of the beat note created at 39.6GHz by photomixing two 1.3μm DFB laser diodes, and the signal frequency at 40GHz. The measurement was taken with a thermal-noise limited receiver as indicated by the flat noise floor. The tail of the beat note in this case lies beneath the thermal noise. As the frequency separation $\omega_D = \omega_{MM} - \omega_B$ is increased or the RF linewidth $\Delta\omega$ of the beat note reduced, the effect of beat-note "spill-over" noise due to the tail is diminished. The difference frequency ω_D is determined solely by the data bandwidth. An analytical expression for the CNR due to the beat-note noise alone is given by [19]:

$$(C/N)_{beat\ note} = \frac{\pi m^2 f_D^2}{2\Delta\nu B} \quad \text{(dB)} \tag{9}$$

where B is the data bandwidth and $f_D = \omega_D/2\pi$; $\Delta\nu = \Delta\omega/2\pi$.

The second noise term is a result of the delay mismatch between the two paths from the coupler to the external modulator. Its effect can be ascertained analytically by taking the Fourier

Transform of the autocorrelation function of the last term in (8). The power-spectral density (per Hz) in the vicinity of the signal is:

$$S(\omega) = 2\pi e^{-\frac{|\tau|}{t_b}} \delta(\omega) + \frac{|\tau|^2}{t_b} \tag{10}$$

where $\Delta\nu = 1/(\pi t_b)$ and assuming that $|\tau| \ll t_b$. Delay mismatch noise appears as a noise pedestal in the band occupied by ω_{MM}. The greater the mismatch, the higher the pedestal. With proper adjustment of τ, the noise pedestal becomes insignificant compared to typical noise levels in fiber optic transmission systems. The CNR due to the delay mismatch noise is then simply given as

$$(C/N)_{delay\ mismatch} = 1/(\Delta\nu|\tau|^2 B) \quad \text{(dB)} \tag{11}$$

Table 1 quantifies, for typical device parameters, the relative contribution of each noise source considered independently. The results reveal that beat-note noise sets the fundamental CNR limit of this technique.

B. Dynamic Range

Dynamic range of the feedforward modulator is considered next. Referring to Figure 10, the input mm-wave mixer sets the upper limit (third-order intercept) of the of the spur-free dynamic range. The lower limit (noise) is determined by the beat-note noise. As discussed above, the beat-note noise is a function of the difference frequency ω_D, between the beat-note frequency ω_B and the center frequency of the signal ω_{MM} to be transmitted. From Table 1, the noise due to the beat note is approximately -140dBc/Hz. A typical third-order intercept power for the mm-wave mixer is 5dBm. Based on these numbers, an estimate of ~100 dB-Hz$^{2/3}$ is obtained for the spur-free dynamic range of the feedforward modulator.

C. System Implementation

Data transmission using this technique is demonstrated with the setup shown in Figure 10 [28]. A beat note at 36.5GHz generated by photomixing two 1.3μm DFB lasers is electrically mixed with the input mm-wave signal which is centered at 39 GHz and is BPSK modulated at 150-300 Mb/s. The resulting IF "error" signal at 39.0 - 36.5 = 2.5 GHz, is fed forward to an external optical modulator, which impresses the BPSK modulated mm-wave carrier at its output. The optical signal out of the feedforward modulator is transmitted through 2.2 km of single-mode optical fiber and detected by a high speed photodiode. BER measurements are done after the signal is downconverted to baseband, amplified, low-pass filtered and sent to the error-rate tester. The system is first adjusted to achieve a BER=10^{-9} at 150Mb/s, with a required optical power at the receiver of -9.8dBm for the thermal-noise limited receiver. To demonstrate transmission at >150 Mb/s, we plot the optical power penalty as a function of bit rate, with BER fixed at 10^{-9}. As shown in Figure 12, an additional 1.2 dBm of optical power is required to transmit at 300 Mb/s. The inset shows the received eye diagram at 300Mb/s at a BER=10^{-9}.

From the above system experiment, it is clear that the photomixed beat note can be easily adjusted to any frequency within a few hundred gigahertz. The maximum carrier frequency in the feedforward transmitter is therefore limited only by the bandwidth of the photodetector (40 GHz in our case). The data rate on the other hand is limited by the electrical bandwidth of the low-frequency external modulator, as discussed earlier. Photodetectors with bandwidths in excess of 100 GHz have been demonstrated and external modulators with bandwidths ≥20 GHz are commercially available. Therefore, gigabit data rates at carrier frequencies >100 GHz is possible. As an example, for transmission of a 5 Gb/s signal centered at f_{MM} =100 GHz one would use an external modulator with a bandwidth of 10 GHz. The beat note should then be adjusted such that $f_B - f_{MM}$ is 5 GHz (to allow for lower and upper sidebands of the data signal).

IV. OPTOELECTRONIC PHASE-LOCKED LOOP

A. Principle and Analysis

In this section, we demonstrate an alternative technique, namely, the use of an optoelectronic phase-locked loop (PLL) in conjunction with a passively mode-locked laser for optical transmission of stable mm-wave signals over a narrow band. The technique involves the use of a single, low-frequency (direct modulation bandwidth < 1GHz) multiple-contact monolithic semiconductor laser, and in principle can be used for lasers passively mode-locked at frequencies extending to 100GHz and beyond.

The experimental set up of the phase-locked loop is illustrated in Figure 13. The passively mode-locked laser (MLL) is a multi-section, quantum-well laser emitting at 850nm with a cavity length of ~810μm, corresponding to a cavity round-trip frequency of 46.8GHz. One of the sections (shorter) forms the saturated absorber, and the longer section provides gain. The mode-locked laser serves as the voltage-controlled oscillator (VCO) to be stabilized by the PLL. Gain (in MHz/V) of the mode-locked laser is characterized first to ascertain its viability as a VCO. The mode-locked laser fundamental frequency versus absorber voltage is measured, and the characteristic is found to linear with a slope of approximately 10-20MHz/V over the range of absorber voltages used in the experiment [18]. Referring to Figure 13, the collimated light from the laser was split into two paths, one providing for optical feedback to control the free-running passively mode-locked linewidth, and the other focused onto a high-speed photodetector. The detected signal is first downconverted to an intermediate frequency, amplified and sent to another mixer for downconversion to baseband. The baseband signal is now the loop error signal. The stability of the reference oscillator was measured to be <-104 dBc/Hz (at 100 kHz offset). The error signal was passed through an active filter (integrator) with a transfer function:

$$(\omega) = -F(0)\left(\frac{j\omega\tau_2 + 1}{j\omega\tau_1 + 1}\right) \tag{12}$$

where $\tau_2 = 45.47 \times 10^{-9}$ s, $\tau_1 = 3.88 \times 10^{-6}$ s, and F(0) = 43dB. All other relevant loop

parameters are itemized in Table 2. The loop filter output was used to control the MLL pulsation frequency by modulating the absorber, thus forming a second-order PLL. With a free-running MLL RF linewidth of $\Delta\nu$=270 kHz, the loop was activated and the measured single side-band (SSB) phase-noise density at 46.8 GHz is shown in Figure 14. The phase noise is approximately -75 dBc/Hz at an offset frequency 100 kHz from the carrier.

The stability of the locked signal is highly dependent on the free-running linewidth $\Delta\nu$ of the MLL fundamental pulsation frequency. With the assistance of optical feedback [29] from the external mirror, we achieved a $\Delta\nu$=30 kHz and observed an improved phase noise of -100 dBc/Hz (at 100 kHz offset) as shown in Figure 15. This is comparable to the lowest phase noise density achieved using hybrid mode-locking at a much lower cavity round-trip frequency [30]. However, it was difficult to maintain lock under this situation due to the stability of the loop in the presence of optical feedback.

For the optoelectronic phase-locked loop to function as a mm-wave optical transmitter, the loop must be able to track the input mm-wave signal to be transmitted. Tracking of the carrier was observed over ~10MHz. Thus, the loop may be used as a narrowband millimeter wave transmitter with data rates $\leq$10 Mb/s. Figure 15 illustrates tracking of the stabilized fundamental frequency over a range of 1 MHz for a second laser passively mode-locked at 41GHz [18].

Stabilization of the MLL using a PLL is only effective if the free-running linewidth $\Delta\nu$ is sufficiently small. Due to the large delay in the loop (20 ns), locking of the mode-locked signal to the external reference was not possible for $\Delta\nu$ >1 MHz. Wider linewidths lead to an increase in $L(f)$ [31]. The fundamental limit to the stability of the mm-wave carrier using this PLL approach can be determined as follows: With lock, the output phase spectral density is given by [32]:

$$\phi_o(f) = S_{\phi_i}(f)|H(f)|^2 + S_n(f)|H(f)|^2 + S_{\phi_{ML}}(f)|1-H(f)|^2 \quad (13)$$

where $S_{\phi_i}(f)$ is the phase noise spectral density of the reference oscillator, $S_n(f)$ represents the single-sided white noise spectral density of the loop error signal and is $2N_o/V_o^2$ [32]. The quantity $2N_o$ is the single-sided white noise at the detector and is predominantly thermal. Thus, $2N_o = 4kTF/R_o$, where F is the noise factor of the receiver and R_o=50Ω. The voltage $V_o = \sqrt{2}(I_{ph} \cdot 50\Omega)$, where I_{ph} is the detected photocurrent. The phase noise of the free-running mode-locked signal is $S_{\phi_{ML}}(f) = \Delta\nu/(\pi f^2)$ .The closed-loop transfer function is

$$(f) = \frac{f_n + j2\xi f f_n}{f_n^2 - f^2 + j2\xi f f}, \quad (14)$$

for an ideal second-order loop with zero loop delay [32]. The frequency f_n is the PLL natural frequency and ξ is the damping. The last two terms in equation (13) represent the SSB phase noise density while the first term represents the locked signal. If we consider the limit imposed by the free-running mode-locked signal linewidth, then the SSB phase noise density is

$$L(f)_{PN} \cong \Delta\nu f^2/\pi f_n^2 \quad , \quad (15)$$

where f is the offset frequency from the carrier. For a typical PLL with f_n=3 MHz, it is necessary to maintain $\Delta\nu$<100 kHz in order that $L(f)$<-110 dBc/Hz at an offset frequency of 100 kHz. For small RF linewidths $\Delta\nu$ and/or offset frequencies very close to the carrier, then the white noise dominates and

$$L(f)_{WN} \cong 2N_o / V_o^2 = \frac{(2kTF)}{\left(RP_o\right)^2 R_o} .$$

For typical values of optical power P_0=0.5 mW; R=0.20 A/W; noise factor F=10; a limit of $L(f)_{WN}$ < -120 dBc/Hz can be achieved.

B. Dynamic Range

Dynamic range for the optoelectronic phase-lock loop is determined by the input mm-wave mixer and the noise under the phase-locked condition. With lock, -100dBc/Hz was obtained with this technique, for a spur-free dynamic range of ~70 dB-$Hz^{2/3}$. This is comparable to the dynamic range measured for resonant modulation. Based on the above analysis, however, a higher dynamic range is possible with careful consideration to minimize loop delay and the free-running mode-locked frequency linewidth.

V. COMPARISON OF TRANSMISSION TECHNIQUES

Table 3 summarizes and compares the results of the three techniques. Resonant modulation is the simplest technique to implement, since it involves the use of only a single, ordinary semiconductor laser. Whether the spur-free dynamic range (SFDR, measured in a 1Hz bandwidth) of resonant modulation and the phase-locked loop results in a performance compromise at the system level depends on the system architecture. As discussed above, dynamic range is not an issue when considering fiber-fed indoor mm-wave picocellular networks, since two channels can be time-multiplexed. On the other hand, in multichannel analog transmission systems, the low dynamic range may limit the number of users. Millimeter wave wireless cable-television systems (with fiber-fed head-end antennas) utilizing FM will substantially alleviate the high dynamic range required for conventional AM systems [33]. The distortion is not a consideration in single-tone systems, where, for example, a mm-wave tone is used to synchronize spatially distributed phased-array antennas. It should be pointed out that the use of a predistortion circuit can increase the dynamic range of the resonant modulation transmitter by 10dBover a narrow band. The feed-forward modulator, although high in component count, is the most flexible mm-wave optical transmitter and offers a dynamic range comparable to that of external modulators and tunability

not possible with the other two techniques. In addition, all components in the feedforward modulator are Optoelectronic Integrated Circuit (OEIC) compatible. For most mm-wave applications, however, the center frequency remains fixed, and a passband bandwidth of several hundred megahertz is usually sufficient. Resonant modulation thus appears to be the optimum choice considering its simplicity.

VI. CONCLUSION

We have presented the implementation and analysis of three novel techniques used to transmit narrowband mm-wave signals over optical fiber. Practical issues such as narrowband matching of the laser at mm-wave frequencies, dynamic range, noise and modulation response were considered in detail for resonant modulation of multiple contact devices. Resonant modulation of single-contact devices was also demonstrated, and can have a significant impact on the design of single monolithic lasers at mm-wave frequencies for both mm-wave signal transmission and ultrahigh frequency mode-locking. A two-channel system implementation of resonant modulation was performed in which two simultaneous users at 41GHz were transmitted over 400meters of optical fiber.

A novel frequency-agile mm-wave transmitter based on feedforward modulation was also implemented. The fundamental limit to the noise and dynamic range was considered, and a system demonstration in which 300Mb/s at 39GHz was transmitted over 2.2km of fiber. Although possessing a high component count, the feedforward modulator provides a high dynamic range and can potentially provide transmission of multi-gigabit data at carrier frequencies beyond 300GHz. All components in the feedforward modulator are OEIC compatible.

Operation of a simple optoelectronic phase-locked loop to stabilize the fundamental frequency of a single, low-frequency quantum-well laser passively mode-locked at mm-wave frequencies was demonstrated. Phaselocking at 46.8GHz to an external reference oscillator resulted in a phase-noise density of -100dBc/Hz. Fundamental limits using this approach was considered. The tracking capability and loop bandwidth was discussed for the phase-locked loop operating as a narrowband mm-wave optical transmitter.

The relative merits of the three techniques were discussed in terms of maximum carrier frequency, passband bandwidth, tunability, dynamic range and degree of complexity. The mm-wave subcarrier transmission results presented in this reportreport the highest reported to date.

References

[1] W.I. Way, "Optical Fiber-Based Microcellular Systems: An Overview," *IEICE Trans. Commun.*, vol. E76-B, no. 9, pp. 1091-1102, Sept. 1993.

[2] H. Ogawa, D. Polifko, S. Banba, "Millimeter-Wave Fiber Optics Systems for Personal Radio Communication," *IEEE Trans. Microw. Theory and Techniq.*, vol. 40, no. 12, pp. 2285-2293, Dec. 1992.

[3] H. Thomas, N. Imai, "Millimeter Waves Over Optical Fiber for Broadband Wireless Communication," *Optical Fiber Conference*, 1994 *(OFC '94)*, report no. TuJ4.

[4] Ta-Shing Chu, "Fiber Optic Microcellular Radio," *IEEE Trans. on Vehicular Techn.*, vol. 40, no. 3, pp. 599-606, Aug. 1991.

[5] J. O'Reilly, P. Lane, "Remote Delivery of Video Services Using mm-Waves and Optics," *IEEE J. Light. Techn.*, vol. 12, no. 2, pp. 369-375, Feb. 1994.

[6] A.S. Daryoush, "Optical Synchronization of Millimeter-Wave Oscillators for Distributed Architectures," *IEEE Trans. Microwave Theory Tech.*, vol. 38, no. 5, pp. 467-476, May 1990.

[7] S. D. Offsey, L. F. Lester, W. J. Schaff, L. F. Eastman, "High-speed Modulation of Strained-Layer InGaAs-GaAs-AlGaAs Ridge Waveguide Multiple Quantum Well Lasers," *Appl. Phys. Lett.*, vol. 58, no. 21, pp. 2336- 2338, 27 May 1991.

[8] D.W. Dolfi and T. Ranganath, "50GHz Velocity-Matched Broad Wavelength $LiNbO_3$ Modulator with Multimode Active Section," *Electron. Lett.*, vol. 28, no. 21, pp. 1197- 1198, 1992.

[9] K. Noguchi, H. Miyazawa, O. Mitomi "75GHz Ti:$LiNbO_3$ Optical Modulator," *Optical Fiber Conference*, 1994 *(OFC '94)*, paper no. WB3.

[10] K.Y. Lau and A. Yariv, "Direct modulation and active mode locking of ultrahigh speed GaAlAs lasers at frequencies up to 18 GHz," *Appl. Phys. Lett.*, vol. 46, no. 4, pp.326-328, Feb. 1985.

[11] R. Nagarajan, S. Levy, A. Mar, and J.E. Bowers, "Resonantly Enhanced Semiconductor Lasers for Efficient Transmission of Millimeter Wave Modulated Light," *IEEE Photon. Tech.*

Lett., vol. 5, no. 1, Jan. 1993.

[12] S. Levy, R. Nagarajan, A. Mar, P. Humphrey and J.E. Bowers, "Fibre-Optic PSK Subcarrier Transmission at 35GHz Using a Resonantly Enhanced Semiconductor Laser," *Electron. Lett.*, vol. 28, no. 22, pp. 2103-2104 Oct. 1992.

[13] K. Y. Lau, "Narrow-band Modulation of Semiconductor Lasers at Millimeter Wave Frequencies (>100 GHz) by Mode Locking," *IEEE Journal of Quantum Electronics*, vol. 26, no. 2, pp. 250-261, Feb. 1990.

[14] K.Y. Lau and J.B. Georges, "On the characteristics of narrow-band resonant modulation of semiconductor lasers beyond relaxation oscillation frequency," *Appl. Phys. Lett.*, vol. 63, no. 11, pp. 1459-1461, Sept. 1993, and "Erratum: On the characteristics of narrow-band resonant modulation of semiconductor lasers beyond relaxation oscillation frequency," *Appl. Phys. Lett.*, vol. 63, no. 22, p.3093, Nov. 29, 1993.

[15] J.B. Georges M.H. Kiang, K. Heppell, M. Sayed and K.Y. Lau, "Optical Transmission of Narrow-Band Millimeter-Wave Signals by Resonant Modulation of Monolithic Semiconductor Lasers," *IEEE Photon. Tech. Lett.*, vol. 6, no. 4, April 1994.

[16] U. Gleise, T.N. Nielsen, M. Bruun, E. Lintz Christensen, K.E. Stubkjaer, S. Lindgren, and B. Broberg, "A wideband Heterodyne Optical Phase-locked Loop for Generation of 3-18GHz Microwave Carriers," *IEEE Photon. Tech. Lett.*, vol. 4, no. 8, pp. 936-938, August 1992.

[17] G.R. Olbright, R.P. Bryan, W.S. Fu, R. Apte, D.M. Bloom, and Y.H. Lee, "Linewidth, Tunability, and VHF-Millimeter Wave Frequency Synthesis of Vertical-Cavity GaAs Quantum-Well Surface-Emitting Laser Diode Arrays," *IEEE Photon. Tech. Lett.*, vol. 3, no. 9, pp. 779-781, September 1991.

[18] L.A. Buckman, J.B. Georges, J. Park, D. Vassilovski J. M. Kahn, and K.Y. Lau, "Stabilization of Millimeter-Wave Frequencies from Passively Mode-Locked Semiconductor Lasers Using an Opto-Electronic Phase-Locked Loop," *IEEE Photon. Tech. Lett.*, vol. 5, no. 10, pp.1137-1140, October 1993.

[19] O.Solgaard, J. Park, J.B. Georges, P.K. Pepeljugoski, K.Y. Lau, "Millimeter Wave, Multigigahertz Optical Modulation by Feedforward Phase Noise Compensation of a Beat Note Generated

by Photomixing of Two Laser Diodes," *IEEE Photon. Tech. Lett.*, vol. 5, no. 5, pp. 574-577, May 1993.

[20] H. Haken and M. Pauthier, "Nonlinear Theory of Multimode Action in Loss Modulated Lasers," *IEEE Journal of Quantum Electronics*, vol. QE-4, no. 7, pp.454-459, July 1968.

[21] J.B. Georges, T.C. Wu, D.M. Cutrer and K.Y. Lau, "Millimeter Wave Optical Transmitter at 45GHz by Resonant Modulation of a Monolithic Tunable DBR Laser," *Accepted for presentation at Conference on Lasers and ElectroOptics (CLEO '95)*, Dec. 1994

[22] J.B. Georges, D.M. Cutrer, and K.Y. Lau, "Theory of Resonant Modulation at Millimeter Wave Frequencies of Inhomogeneously Biased Monolithic Quantum Well Lasers," *To appear in IEEE Photon. Tech. Lett.*, March 1995.

[23] K.Y. Lau, P.L. Derry and A. Yariv, "Ultimate limit in low threshold quantum well GaAlAs semiconductor lasers," *Appl. Phys. Lett.*, vol. 52, no. 2, pp. 88-90, Jan. 1988.

[24] D.M. Cutrer, J.B. Georges, Tuan H. Le, and K.Y. Lau, "Dynamic Range Requirements for Optical Transmitters in Fiber-Fed Microcellular Networks," *Submitted to Photonics Technology Letters*, Dec. 1994

[25] J.B. Georges, D.M. Cutrer, M.H. Kiang, and K.Y. Lau, "Multichannel Millimeter Wave Subcarrier Transmission by Resonant Modulation of Monolithic Semiconductor Lasers," *IEEE Photon. Tech. Letters*, March 1995.

[26] D.A. Tauber, R. Spickermann, R. Nagarajan, T. Reynolds, A Holmes Jr. and J.E.Bowers, "Inherent bandwidth limits in semiconductor lasers due to distributed microwave effects," *Applied Phys. Lett.*, vol. 64, no. 13, pp. 1610-1612, March 28, 1994.

[27] D.M. Cutrer, J.B. Georges, T.C. Wu, B. Wu and K.Y. Lau, "Efficient Modulation of Single Contact Monolithic Semiconductor Lasers at Millimeter Wave Frequencies," *Submitted to Applied Physics Letters*, Jan. 1995.

[28] J.B. Georges, J. Park, O. Solgaard, P. Pepeljugoski, M. Sayed and K.Y. Lau, "Transmission of 300Mb/s BPSK at 39GHz using feedforward optical modulation," *Electron. Lett.*, vol. 30, no. 2, pp. 160-161, Jan. 1994.

[29] O.Solgaard and K.Y. Lau, "Optical Feedback Stabilization of the Intensity Oscillations in Ultrahigh-Frequency Passively Modelocked Monolithic Quantum-Well Lasers," *IEEE Photon. Tech. Lett.*, vol. 5, no. 11, pp. 1264-1267, Nov. 1993.

[30] D.J. Derickson, P.A. Morton, and J.E. Bowers, R.L. Thoson, P.A. Morton, and J.E. Bowers, R.L. Th in external cavity mode-locked semiconductor lasers." *Applied Phys. Lett.*, vol. 59, no. 26, pp. 3372-3374, Dec. 23, 1991.

[31] J.B. Georges, L. Buckman, D. Vassilovski, J. Park, M.H. Kiang, O. Solgaard and K.Y. Lau, "Stable Picosecond Pulse Generation at 46GHz by Modelocking of a Semiconductor Laser Operating in an Optoelectronic Phaselocked Loop," *Electronics Letters.*, vol. 30, no. 1, pp.69-70, Jan. 1994.

[32] F.M. Gardner, *Phaselock Techniques*, 2nd Edition., N.Y., Wiley, 1979.

[33] B. Bossard, "Get Ready for Cellular TV," *Telephone Engineer and Management Magazine*, August 15, 1993.

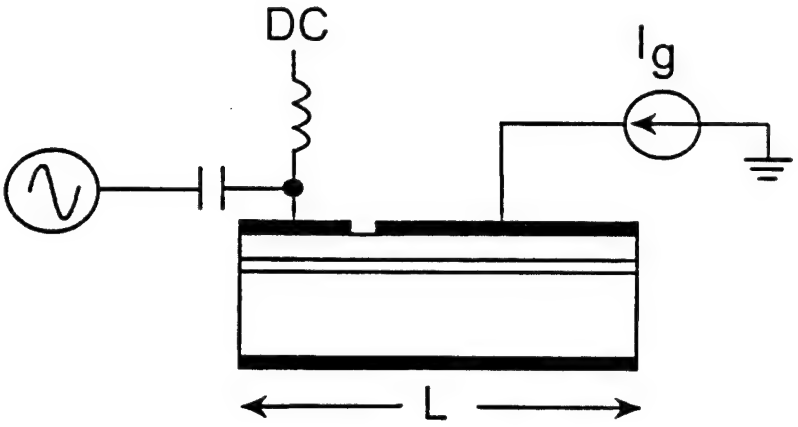

(a)

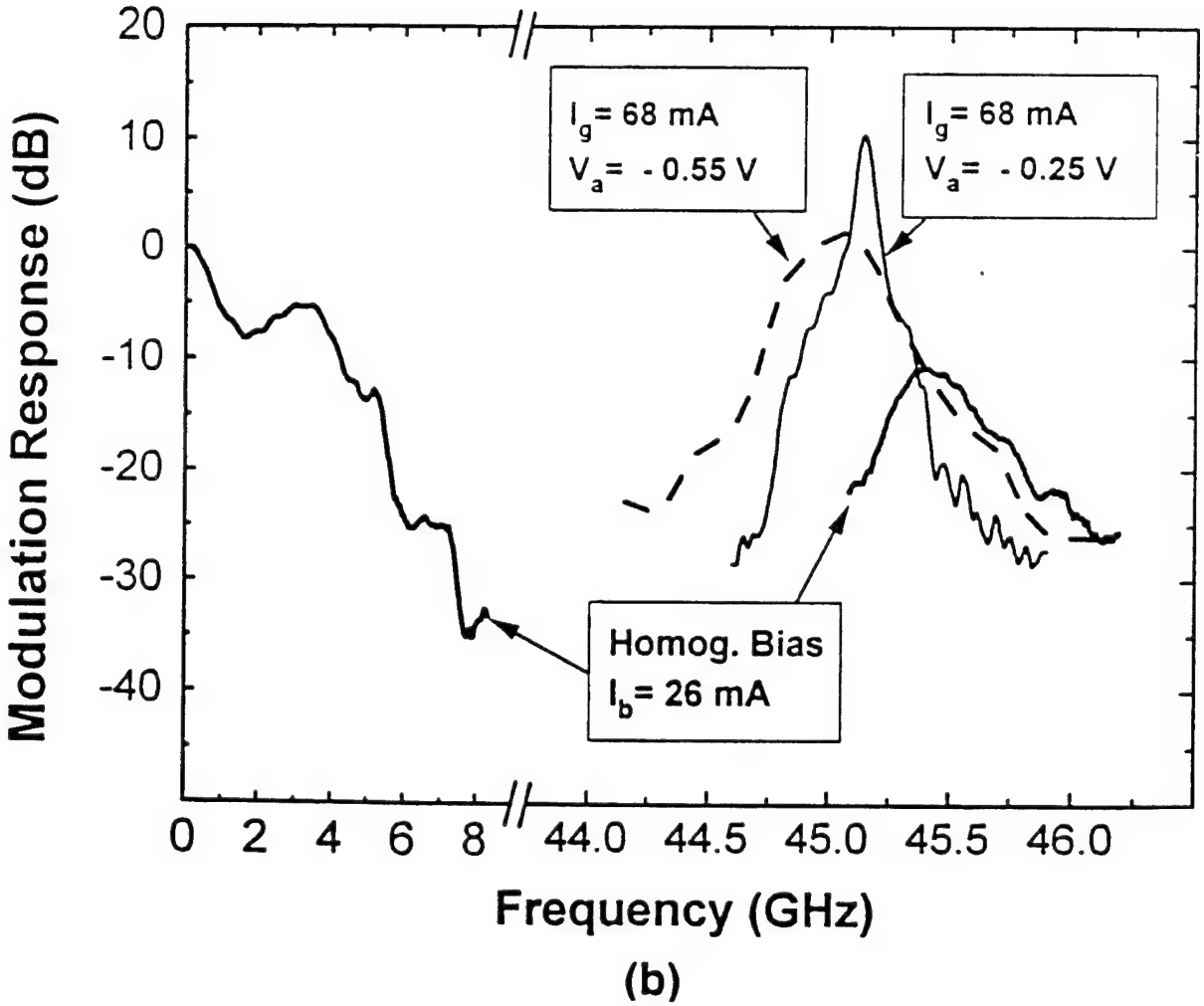

(b)

Figure 1. (a) Monolithic semiconductor laser of cavity length L. Modulation is applied to only a part of the laser cavity. (b) Measured low and high-frequency modulation response of the monolithic semiconductor laser in (a) at a cavity round-trip frequency of 45GHz.

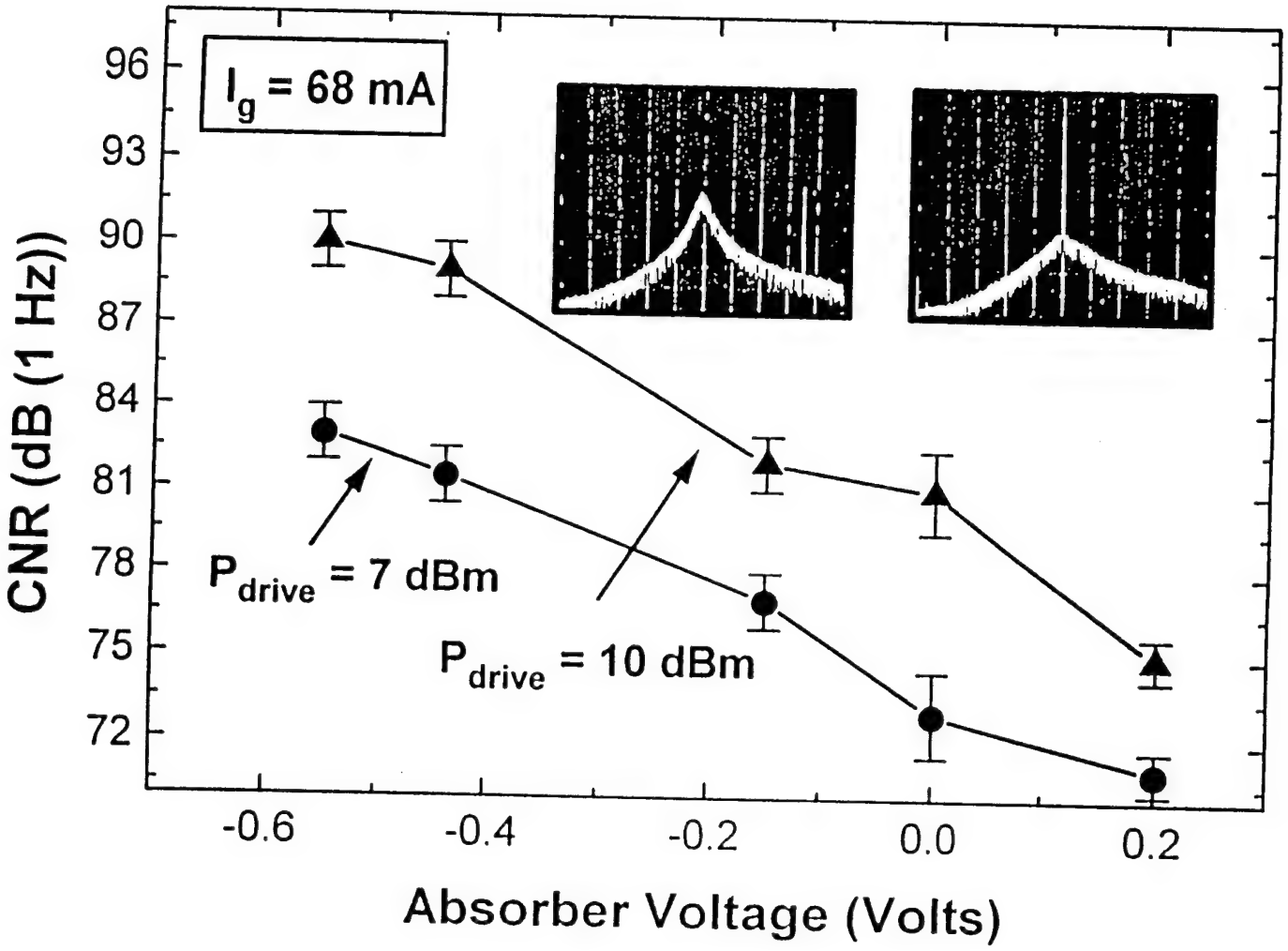

Figure 2. Measured CNR (at 1MHz offset) vs. absorber voltage at a fixed gain-section current of I_g=68mA. The inset illustrates the suppression of the noise at 45GHz due to an applied modulation signal. The scale for the inset is 5dB/div.

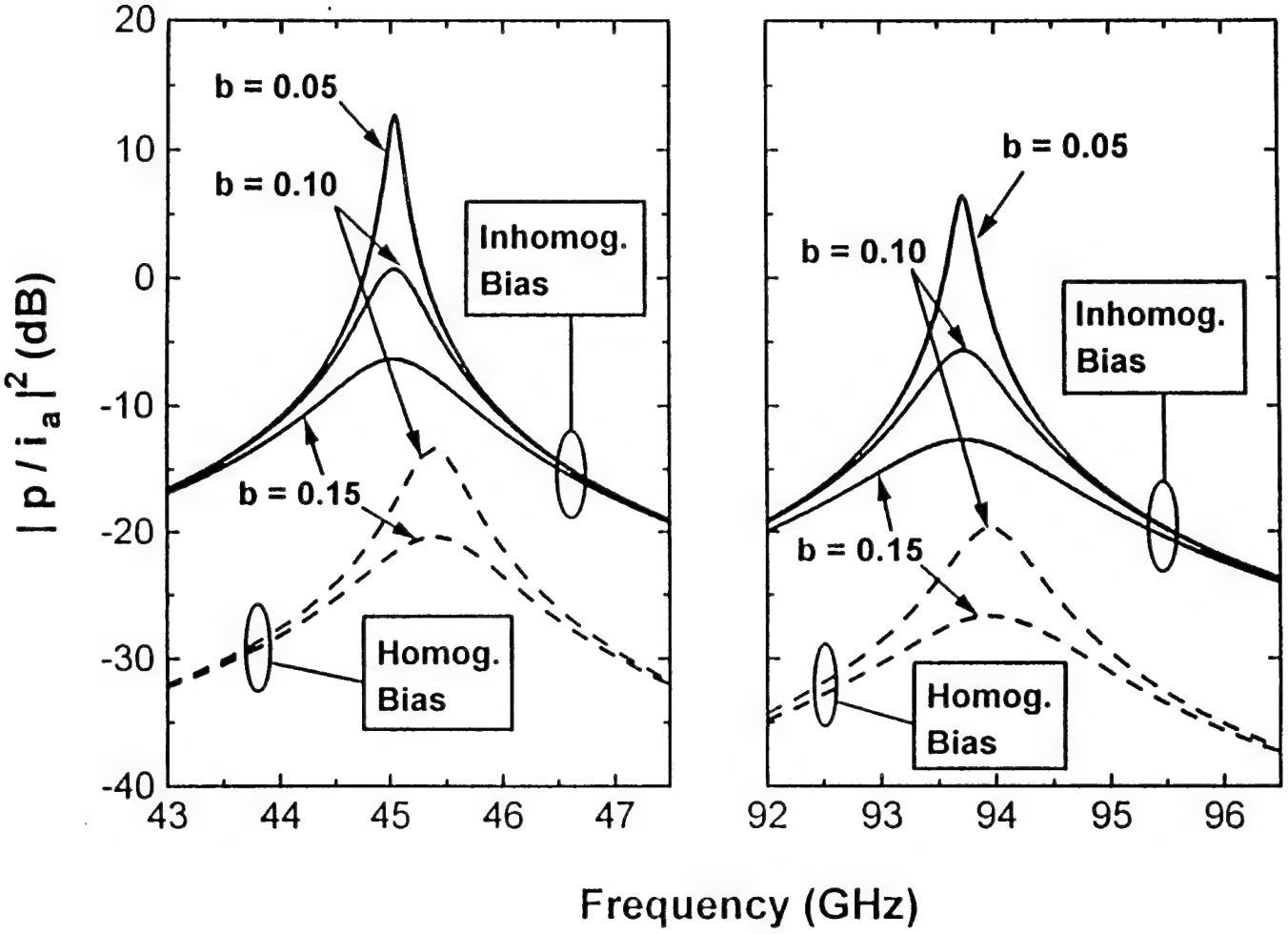

Figure 3. Theoretical bandpass modulation transfer functions plotted for cavity round-trip frequencies at 45 and 94GHz. The plots at 94GHz are for the same bias conditions as those at 45GHz. All response functions are normalized to the modulation efficiency below relaxation oscillation (at d.c.). The parameters for the inhomogeneously biased response functions are a total cavity length L = 825μm; an absorber length L_a = 200μm; τ_p = 3ps; overlap integral for the absorber and gain of $\xi_a = \xi_g$ = 0.22; $\tau_g = \tau_a$ = 2ns. The unsaturated gain g_0=25 and loss a_0=5. The homogeneous response is plotted for τ_{stim} = 0.5ns, τ_s = 2ns and $G = 1.5 \cdot 10^{-12}$ m^3/s. At 94GHz, L = 400μm and L_a = 100μm.

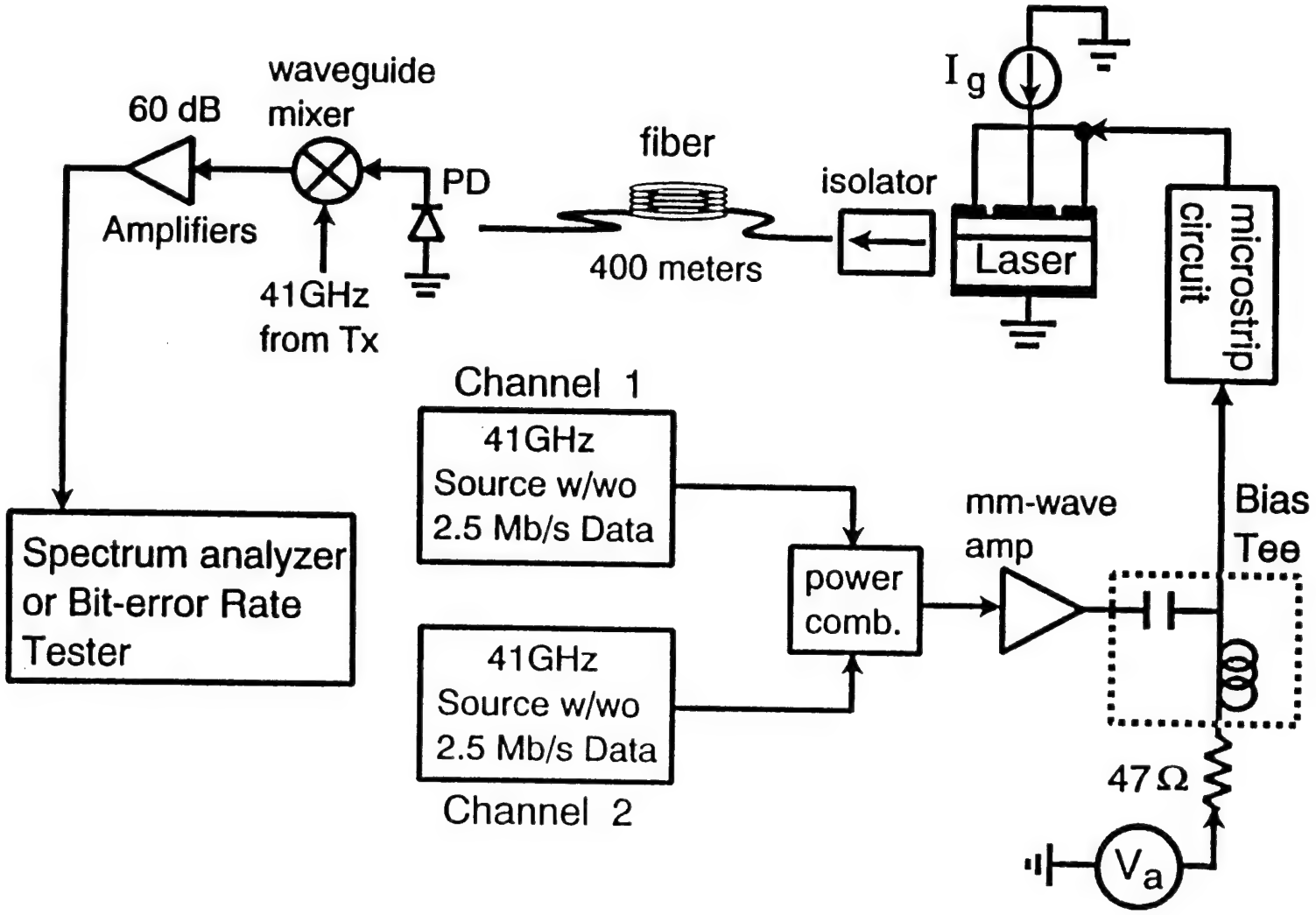

Figure 4. Setup to measure the modulation response for a laser with a cavity round-trip resonant frequency of 41GHz, perform two-tone measurements, and characterize the digital performance of the transmitter.

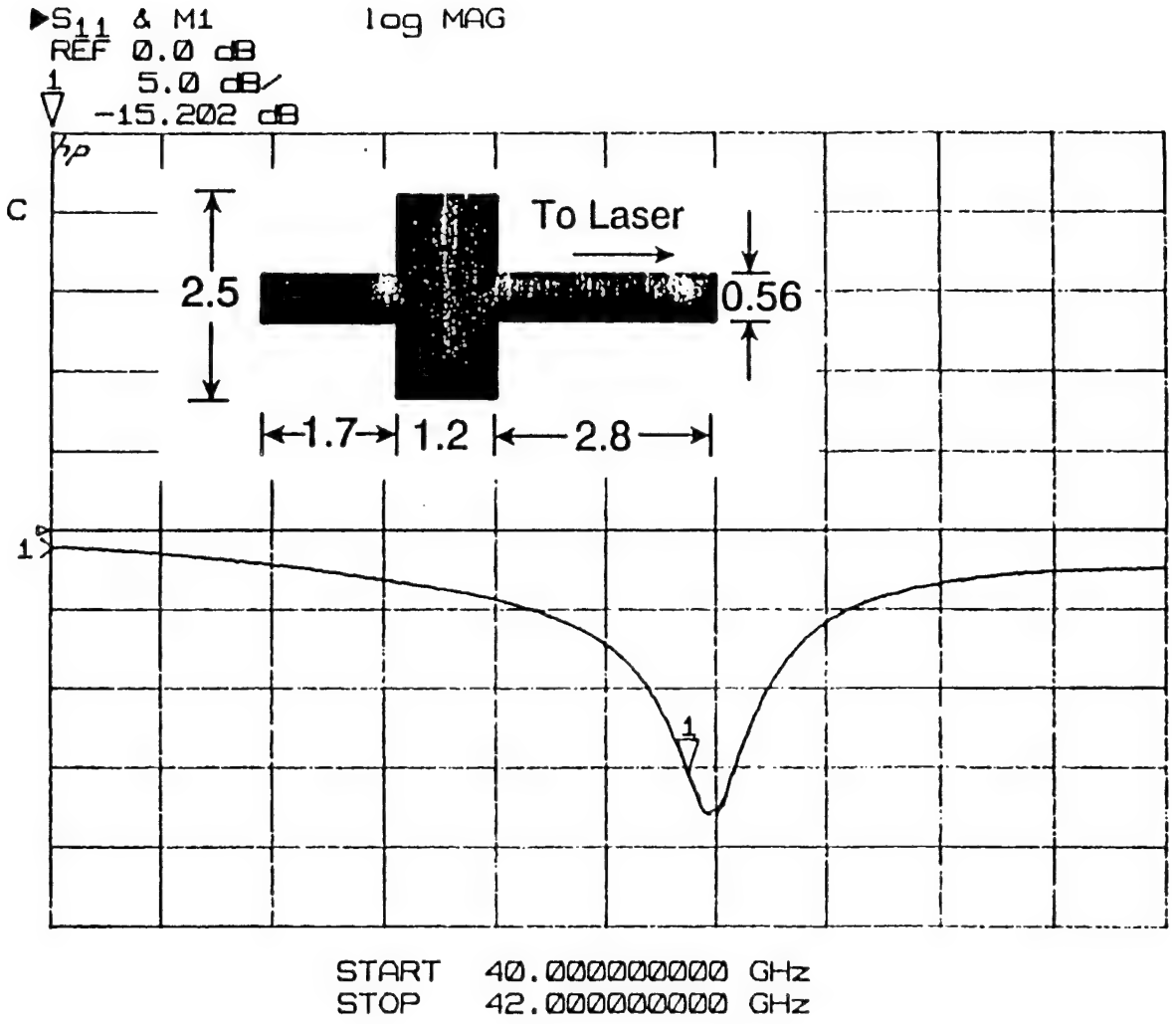

Figure 5. Measured reflection coefficient S_{11} of the combined laser plus matching circuit. The matching circuit was fabricated on a 0.18mm thick Duroid board with metallization dimensions (in millimeters) shown in the inset.

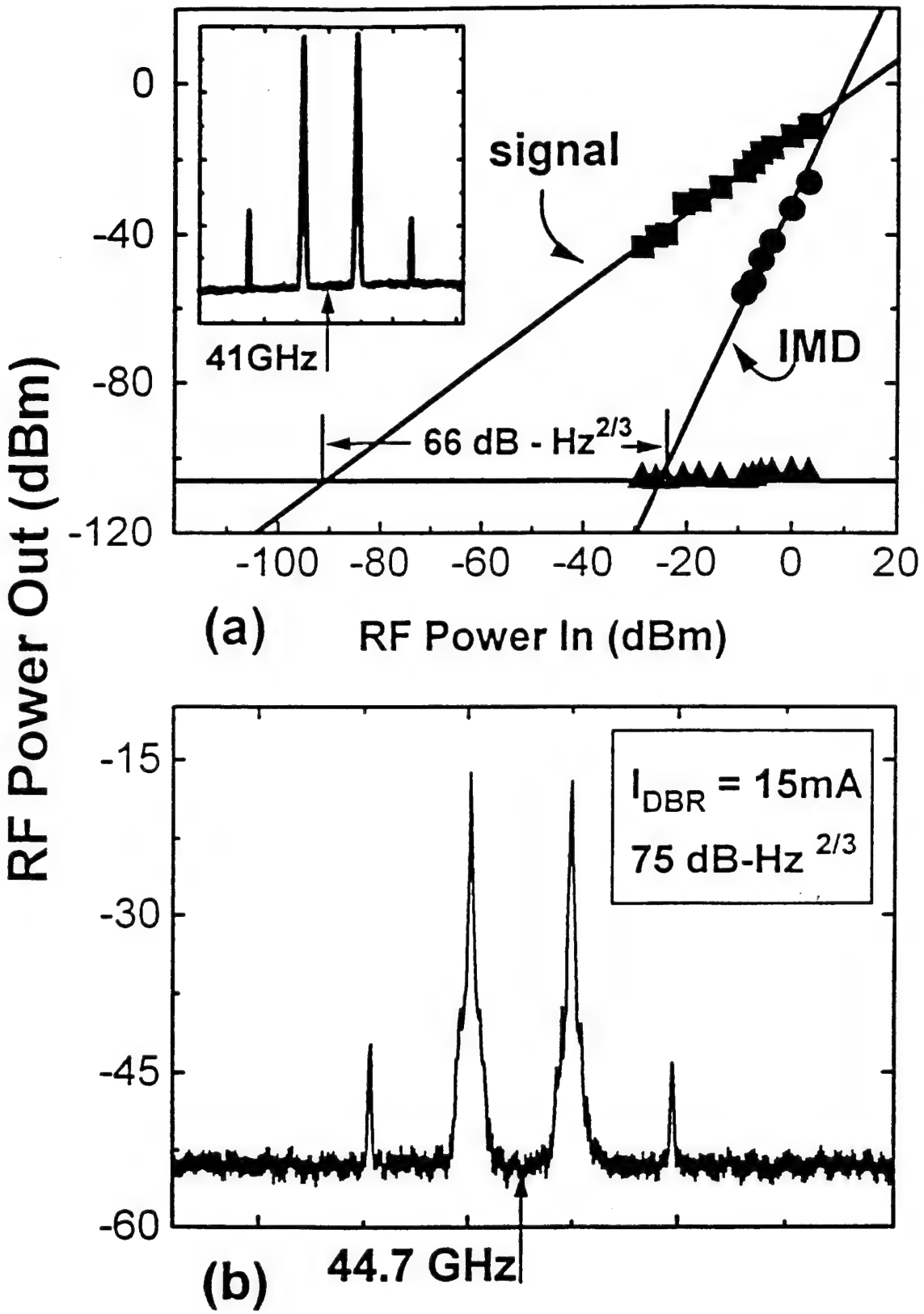

Figure 6. (a) Measured two-tone dynamic range for a modulation efficiency of (a) 0dB at 41GHz. The scale for the inset is 5dB/div. (b) Two-tone plot for a spur-free dynamic range of 75dB-$Hz^{2/3}$ of a 3-section DBR laser described in Ref. [21].

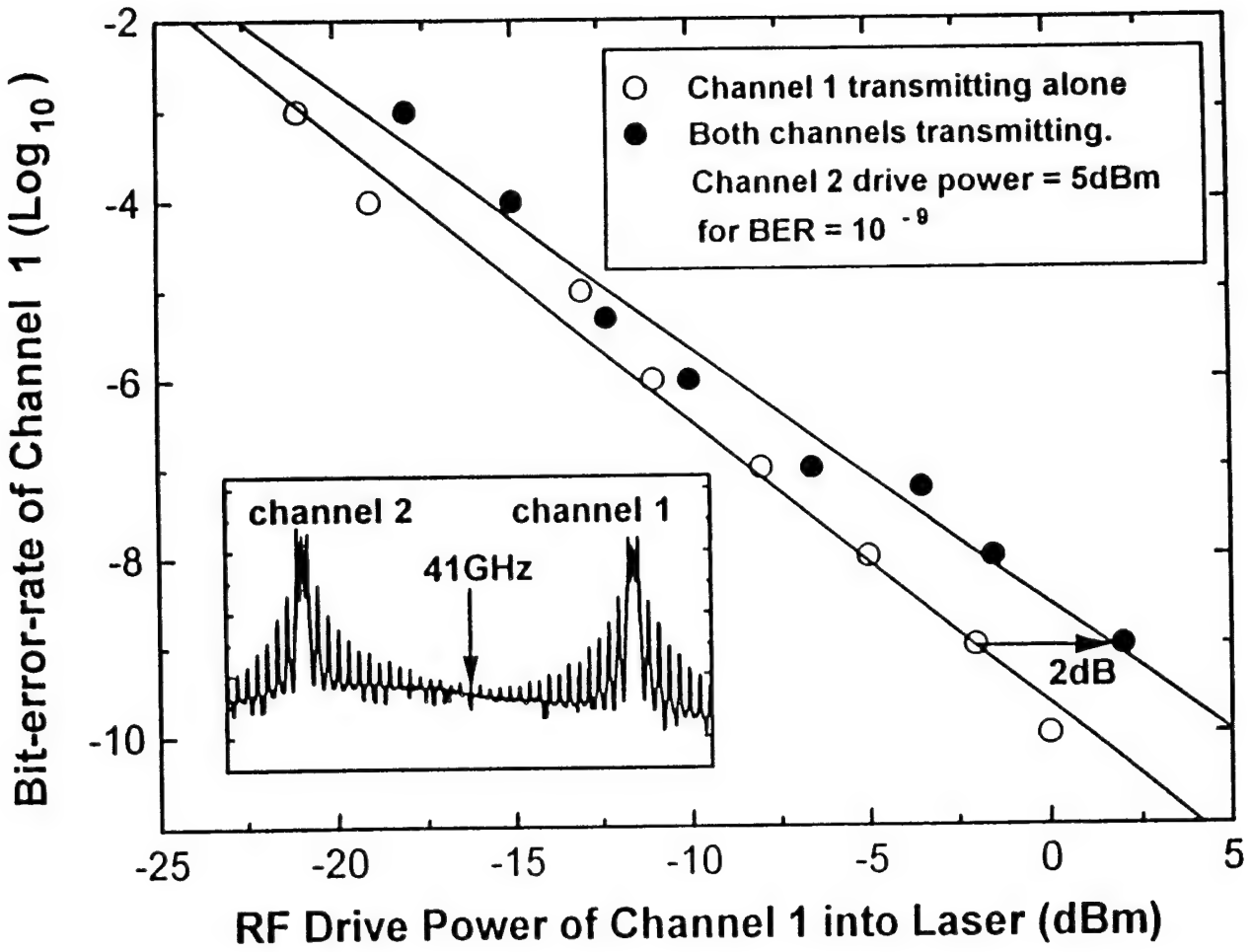

Figure 7. Bit-error rate of channel 1 as a function of RF drive power of channel 1 with and without the presence of channel 2 for 2.5Mb/s return-to-zero BPSK modulation centered around 41GHz. The inset shows the received RF spectrum of both channels transmitting simultaneously after transmission over 600 meters of single-mode fiber. The inset scale is 5dB/div.

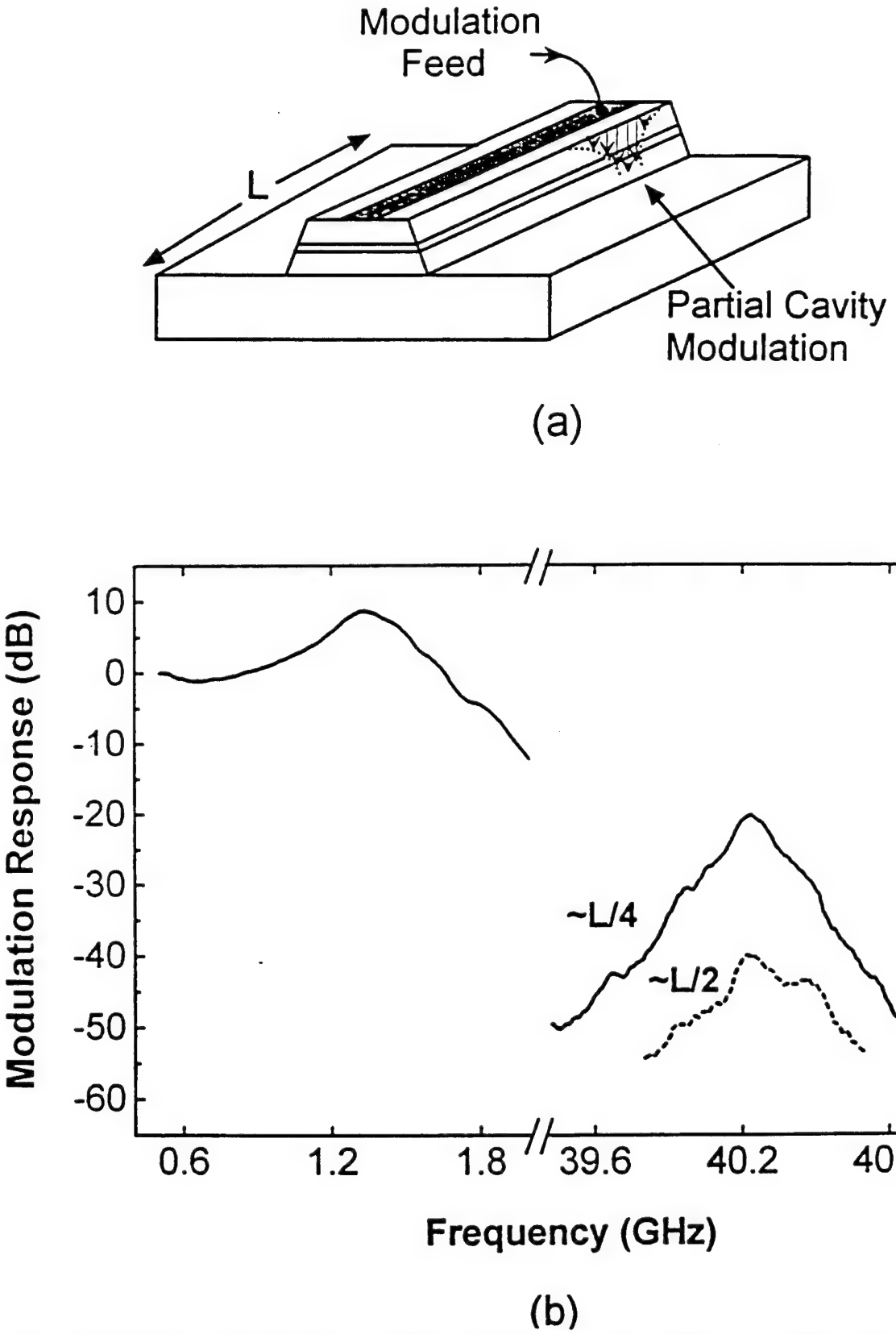

Figure 8. Illustration of the principle of resonant modulation and mode-locking of a single-contact monolithic semiconductor laser. (**a**) The microwave propagation loss of the applied modulation current at the round-trip cavity frequency results in partial cavity modulation and eliminates the need for a second contact. (**b**) Measured modulation response in the low and high frequency range when the modulation feed is positioned at *L/4* and *L/2* along the laser contact.

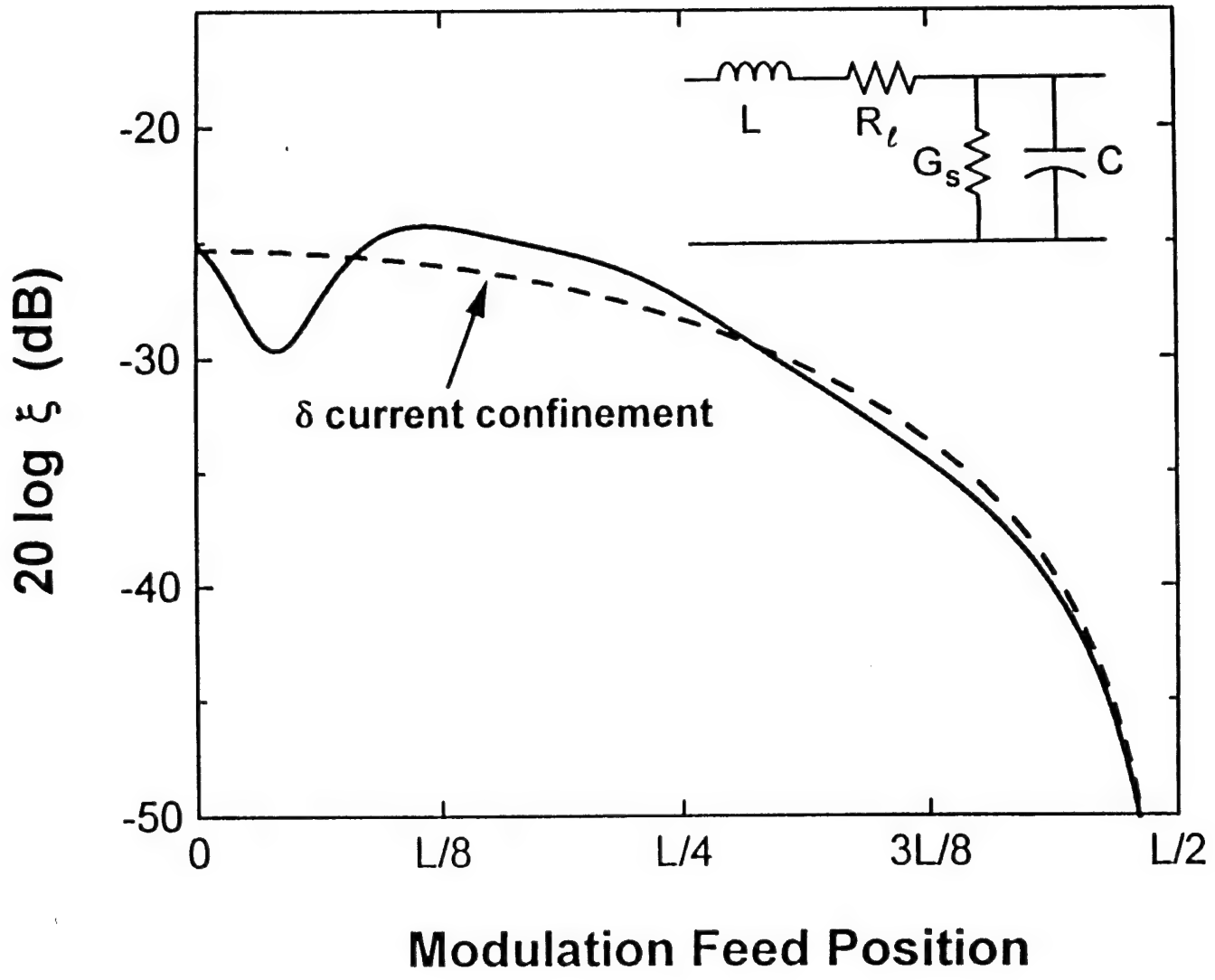

Figure 9. Spatial overlap integral for the laser modeled as an open-ended transmission-line shown in the inset. The values for the transmission line circuit elements are taken from Ref. [26].

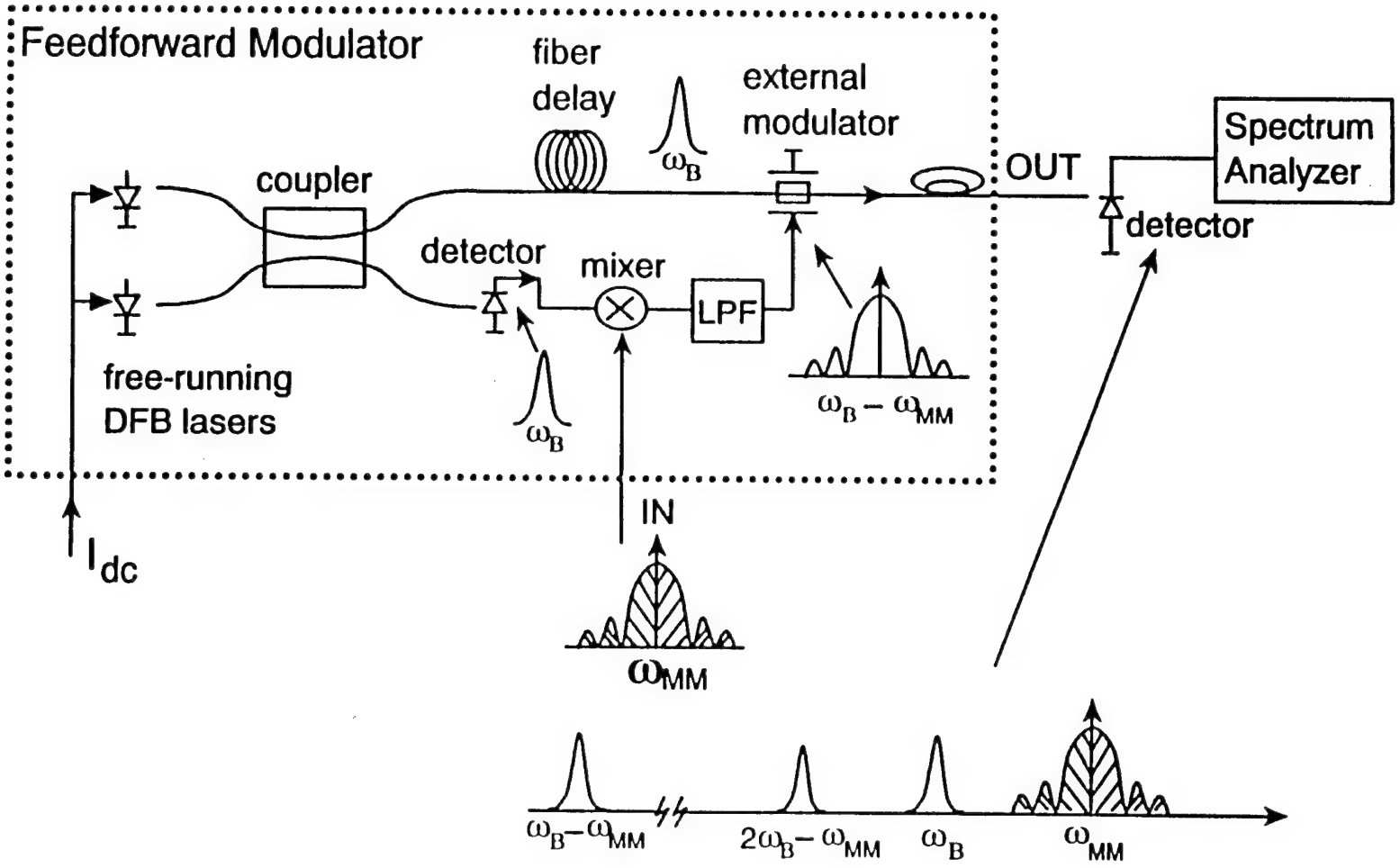

Figure 10. Schematic of the feedforward modulator. Also shown is the noise and signal terms out of the feedforward modulator. The setup was used to transmit 300Mb/s data centered at 39GHz and perform bit-error-rate measurements.

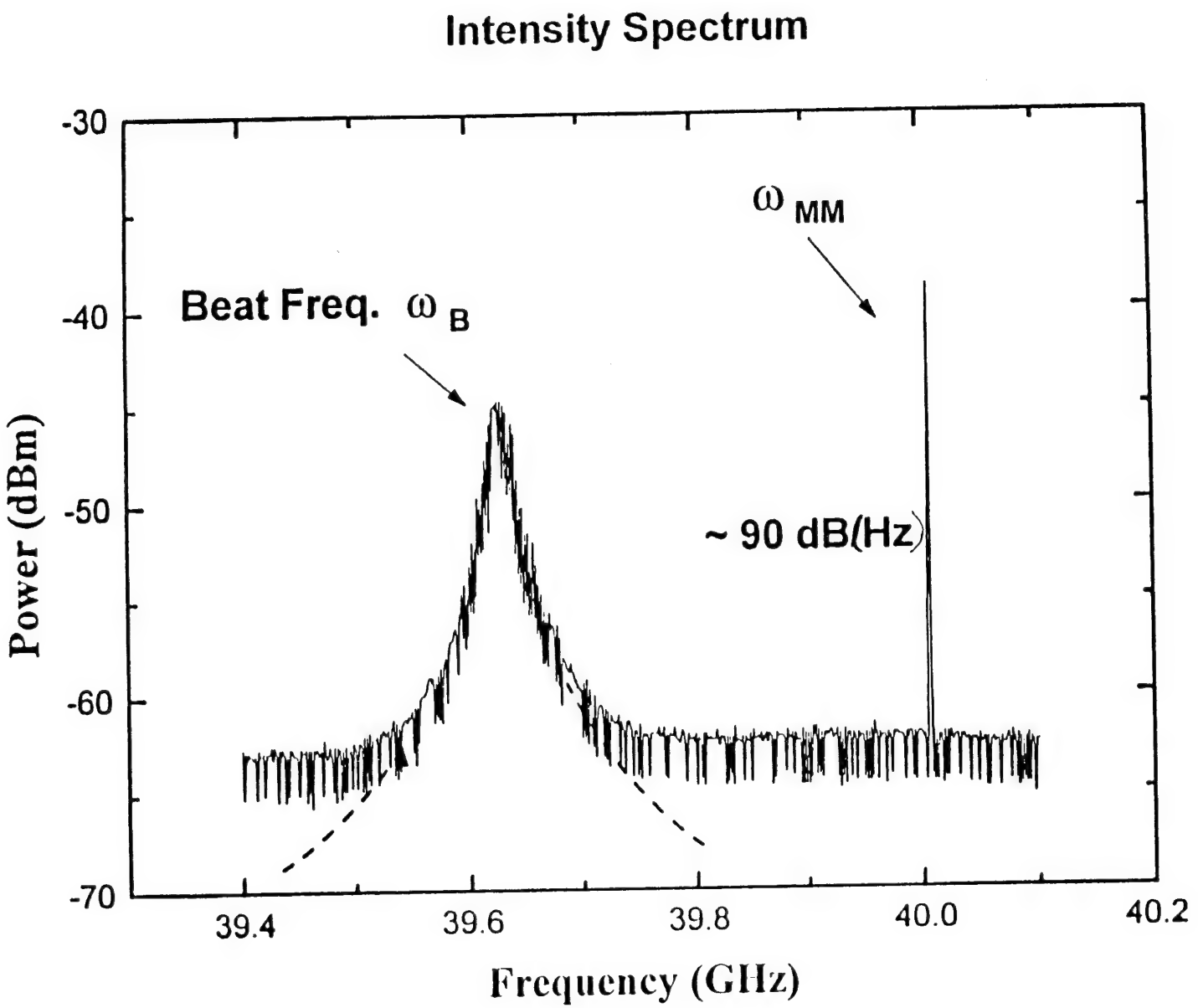

Figure 11. Measured beat note and mm-wave oscillator tone at 40GHz using a thermal-noise limited receiver. Note the tails of the beat note extend below the thermal-noise limit and set the fundamental limit to the CNR for the feedforward modulator.

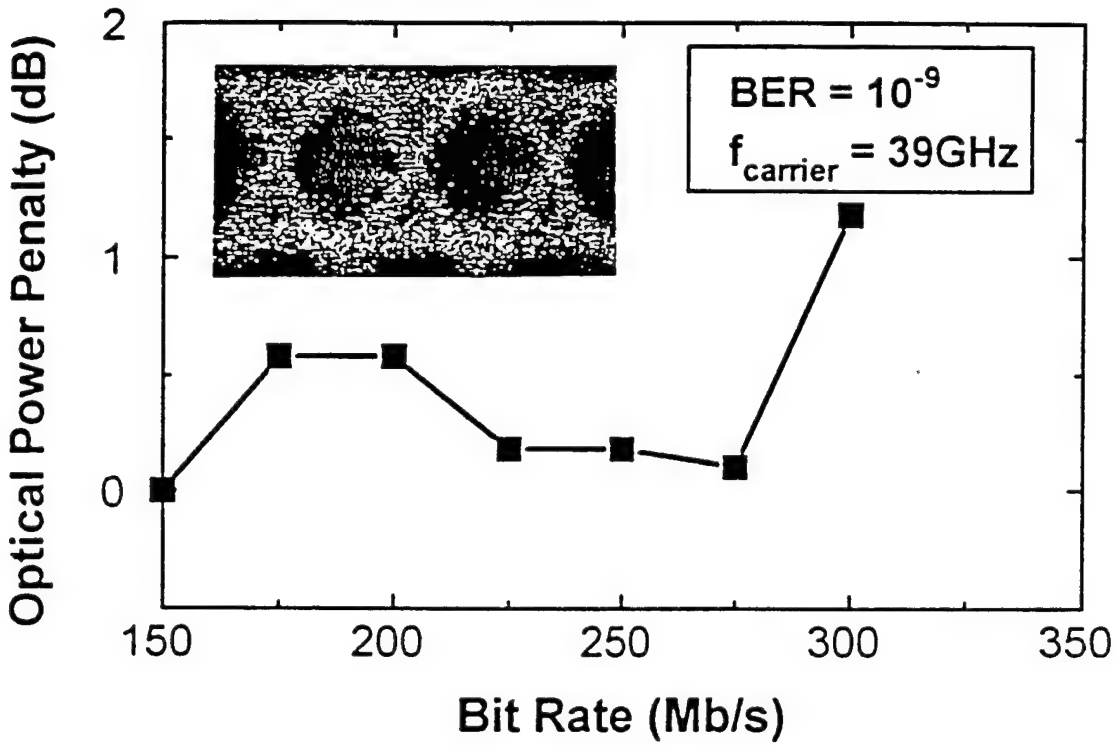

Figure 12. Optical power penalty as a function of bit rate maintaining BER=10^{-9}. The optical power is normalized to that required for transmission at 150Mb/s at a BER=10^{-9}. The inset shows the eye diagram at 300Mb/s.

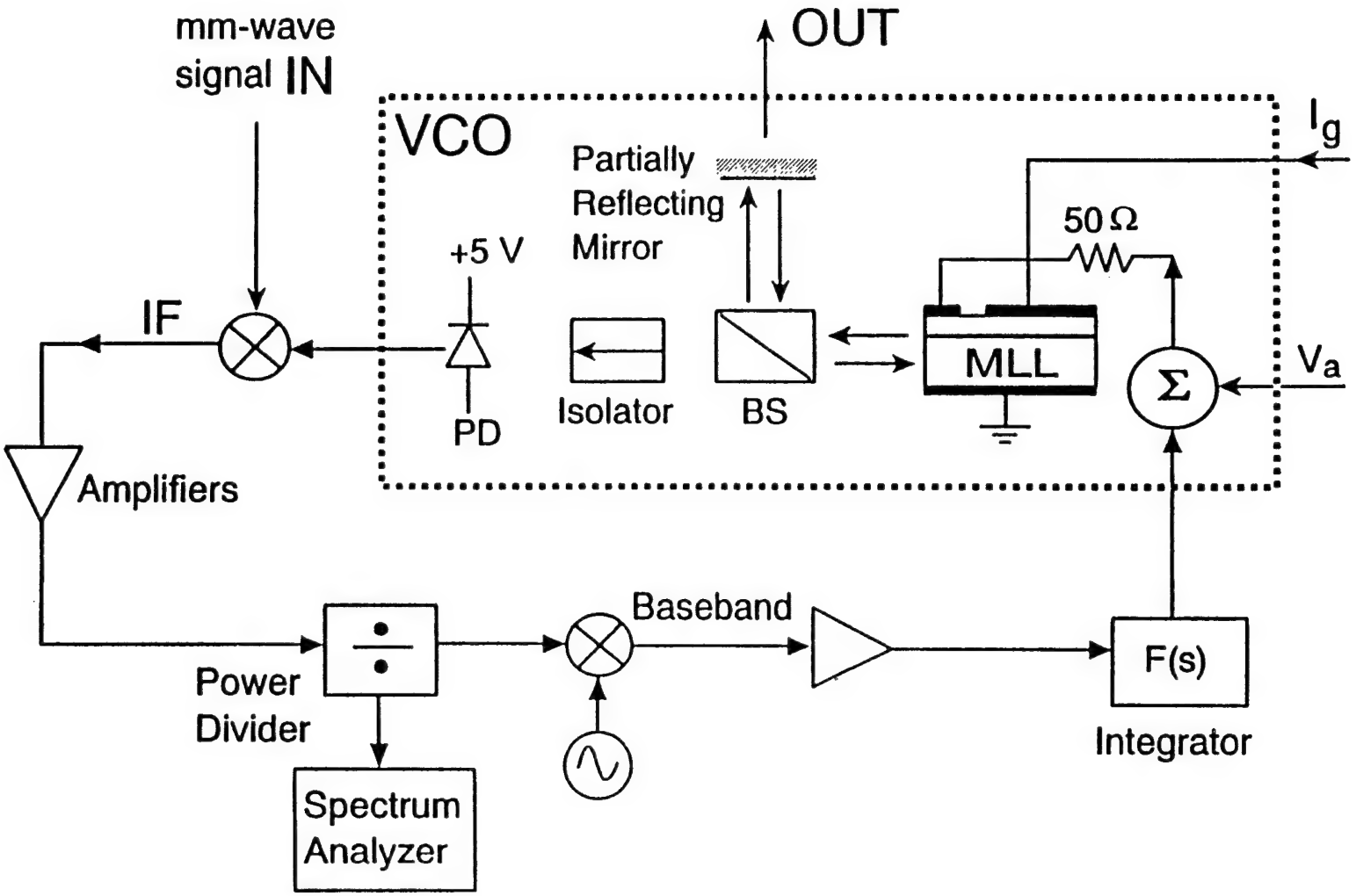

Figure 13. Schematic of the optoelectronic phase-locked loop used to stabilize the fundamental frequency of a passively mode-locked laser at 46.8GHz.

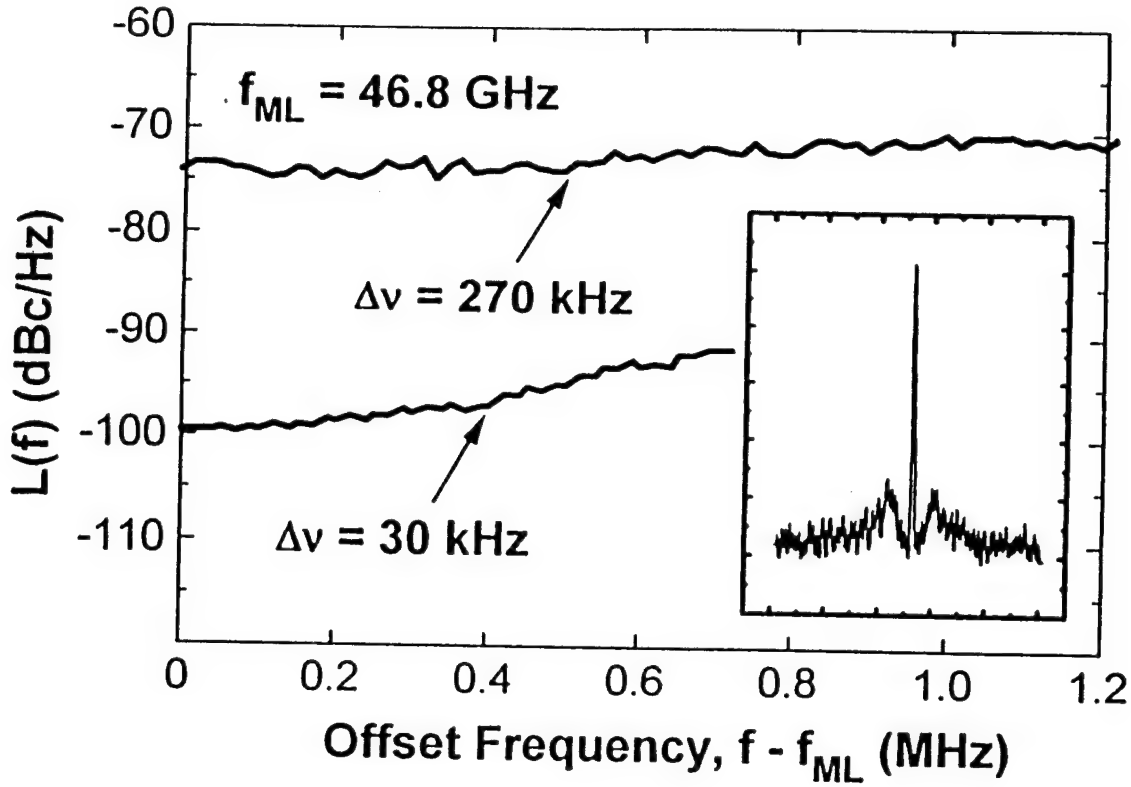

Figure 14. Single sideband phase noise density as a function of offset frequency from the 46.8GHz carrier. The inset shows the locked spectrum for a Δν = 30 kHz.

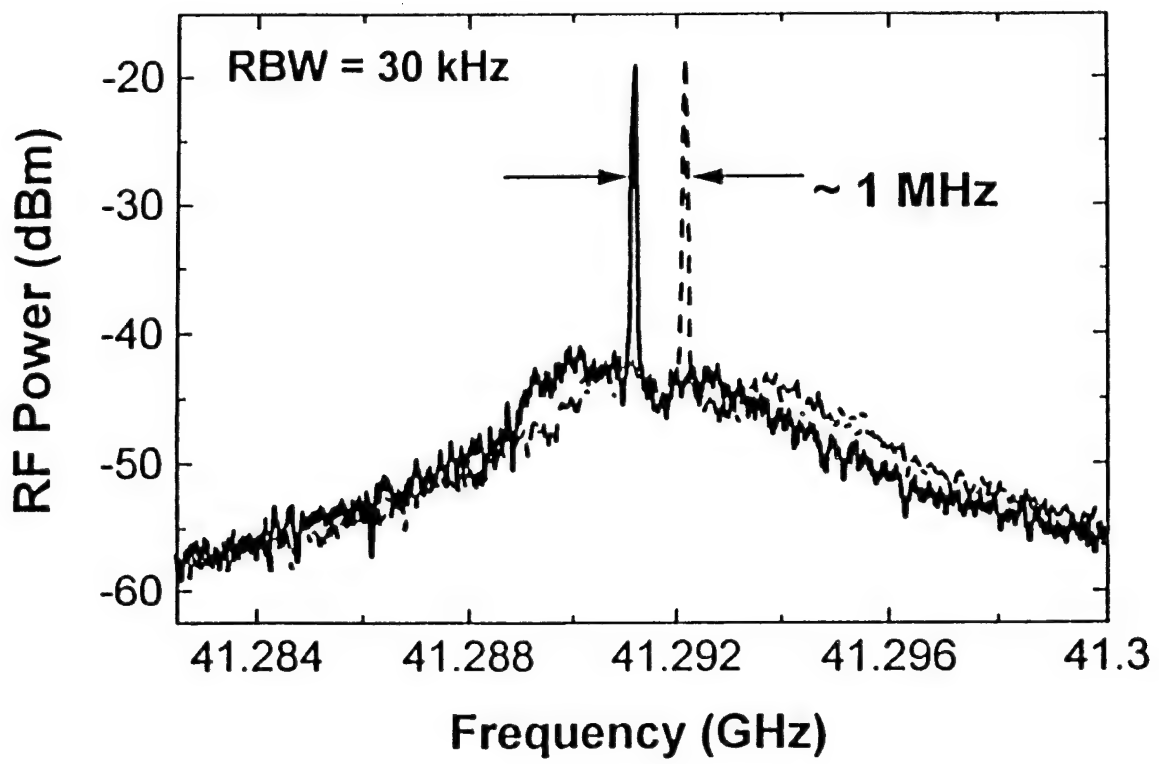

Figure 15. Illustration of tracking of the phase-locked signal as the reference oscillator is tuned over ~1MHz.

Table 1

$\Delta\nu$	τ	$(C/N)_{beat}$	$(C/N)_{delay}$
1 MHz	1 ps	140 dB (1Hz)	180 dB (1Hz)
10 MHz	10 ps	130 dB (1Hz)	150 dB (1Hz)

Table 1. Table illustrating the relative contribution of each noise source unique to the feedforward modulator for an external modulator electrical bandwidth of 8GHz (f_D=8GHz), and a beat-note modulation depth m=1.

Table 2

Loop Parameter	Symbol	Value
Loop Bandwidth	f_z	1.3 MHz
Loop Gain	K	1.4×10^9 rad/s
Damping Coefficient	ζ	0.44
Natural Frequency	ω_n	19 Mrad/s
Loop Delay	τ_d	~ 20ns
MLL RF Linewidth	$\Delta\nu$	770 kHz
Absorber Voltage	V_a	-0.63 V
Gain Current	I_g	52.9 mA
Phase-Error Variance	σ_ϕ^2	0.45 rad^2

Table 2. Summary of phase-locked loop parameters.

Table 3

Technique	$f_{carrier}$	Bandwidth	Tunability	SFDR(dB)	Degree of Complexity
Resonant Modulation	≤ 100GHz	≤ 1GHz	None	≤ 75	Low
Feedforward Modulation	≤300 GHz	≤ 20GHz	≤ 300 GHz	≥ 100	High
Phase-locked Loop	≤ 100GHz	< 10MHz	None	≥ 70	Moderate

Table 3. Comparison of the three mm-wave optical transmitters.

DISTRIBUTION LIST

Addressee	Number of copies
DR. RICHARD A. SOREF ROME LABORATORY-ERDC 80 SCOTT DRIVE HANSCOM AFB, MA 01731-2909	5
ROME LABORATORY/SUL TECHNICAL LIBRARY 26 ELECTRONIC PKY ROME NY 13441-4514	1
ATTENTION: DTIC-OCC DEFENSE TECHNICAL INFO CENTER 8725 JOHN J. KINGMAN ROAD, STE 0944 FT. BELVOIR, VA 22060-6218	2

MISSION

OF

ROME LABORATORY

Mission. The mission of Rome Laboratory is to advance the science and technologies of command, control, communications and intelligence and to transition them into systems to meet customer needs. To achieve this, Rome Lab:

a. Conducts vigorous research, development and test programs in all applicable technologies;

b. Transitions technology to current and future systems to improve operational capability, readiness, and supportability;

c. Provides a full range of technical support to Air Force Materiel Command product centers and other Air Force organizations;

d. Promotes transfer of technology to the private sector;

e. Maintains leading edge technological expertise in the areas of surveillance, communications, command and control, intelligence, reliability science, electro-magnetic technology, photonics, signal processing, and computational science.

The thrust areas of technical competence include: Surveillance, Communications, Command and Control, Intelligence, Signal Processing, Computer Science and Technology, Electromagnetic Technology, Photonics and Reliability Sciences.